Vietnam Journal of Earth Sciences, 47(3), 355–375, https://doi.org/10.15625/2615-9783/23225

Vietnam Journal of Earth Sciences
https://vjs.ac.vn/index.php/jse

Recent monogenic volcanism in North Central Vietnam: Implications for the regional mantle geodynamics

Le Duc Anh[1], Nguyen Hoang[1]*, Tran Thi Huong[1,2], Ryuichi Shinjo[3,4], Le Duc Luong[1], Dang Hoai Nhon[5], Pham Ngoc Can[1]

[1]*Institute of Earth Sciences, VAST, Hanoi, Vietnam*
[2]*Hanoi University of Geology and Mining, Hanoi, Vietnam*
[3]*Research Institute for Humanity and Nature (RIHN), Motoyama 457-4, Kamigamo, Kita-ku, Kyoto 603-8047, Japan*
[4]*Department of Physics and Earth Sciences, University of the Ryukyus, Senbaru-1, Nishihara, Okinawa 903-0213, Japan*
[5]*Institute of Science and Technology for Energy and Environment, VAST, Hanoi, Vietnam*

Received 16 March 2025; Received in revised form 18 April 2025; Accepted 28 July 2025

ABSTRACT

Pliocene to Pleistocene monogenic basalt volcanism in North Central Vietnam is typical of the East and Southeast Asian' diffuse igneous province'. Exposed at Khe Sanh (4.5 Ma), Gio Linh (1.5–1.3 Ma), and Con Co Island (0.35 Ma) the Miocene activity marks the southeastern tip of the Red River Shear Zone (RRSZ) and appears to relate to the rifting of the Hue Sub-basin, triggered by the Song Ca-Rao Nay Fault system (SCRNFS). Petrological analysis of primitive samples suggests that their formation occurred via decompression melting of spinel peridotite mantle at temperatures of 1350–1400°C and pressures of 15–29 kbar. The basalts display oceanic island basalt (OIB)-type geochemical signatures, characterized by enrichment in radiogenic isotopes of Sr, Nd, Pb, and Hf. They are relatively high in TiO_2 and K_2O, and incompatible element concentrations. These suggest a fertile, spinel-peridotite source, influenced by *in situ* metasomatism and/or the presence of recycled subducted oceanic sediment melt. Given the lack of evidence for mantle plume activity beneath the region, we propose that North Central Vietnamese monogenic volcanism reflects decompression melting of a hotter-than-average (Tp ≈ 1400°C) mantle, triggered by lithospheric stretching (greater than 1.5) within the Red River and Hue Sub-basins. In the context of previous regional studies of east/southeast Asian Cenozoic volcanism, Dupal-like mantle affinity is ascribed to eastward asthenospheric flow from the Neo-Tethyan mantle following its closure due to the India-Eurasia collision in the Tertiary.

Keywords: North Central Vietnam, monogenic volcanism, enriched mantle, lithosphere stretching, mantle heterogeneity.

1. Introduction

The Southeast Asia-East Vietnam Sea region lies at the convergence of four major tectonic plates: the Eurasian, Indian, Philippine, and Pacific plates. This complex junction has undergone significant tectonic evolution since the early Cenozoic, primarily driven by the Indo-Eurasian collision that began approximately 55 million years ago.

*Corresponding author, Email: nghoang@ies.vast.vn

This collision initiated a large-scale deformation system extending southeastward, resulting in the formation of continental-scale shear zones, intraplate extensional regimes, and post-collisional basins, including the Gulf of Tonkin and the East Vietnam Sea (EVS) (Tapponnier et al., 1982; 1990).

A central feature of this tectonic network is the RRSZ, a prominent NW-SE trending left-lateral strike-slip fault separating the Indochina and South China blocks. Together with the Song Hong (Red River) Basin (RRB), the RRSZ has played a pivotal role in shaping the regional geodynamic framework. During the Oligocene to Middle Miocene, the RRSZ underwent significant left-lateral displacement, estimated at 500–700 km, which coincided with the rifting and opening of the EVS (Tapponnier et al., 1990; Fyhn et al., 2020). This tectonic regime influenced both sedimentation patterns and structural evolution in the RRB.

Post-Miocene geodynamic activity in Vietnam's North Central region is marked by widespread intraplate volcanism. Pliocene-Holocene basaltic fields, primarily composed of subalkaline olivine-bearing basalts, are distributed along reactivated NW-SE and NE-SW trending fault zones (Rangin et al., 1995; Richard et al., 2024). These basalts typically form monogenic volcanic cones, often emplaced over older Miocene basaltic layers, indicating episodic volcanic activity interspersed with quiescent intervals (Hoang and Flower, 1998; Hoang et al., 2021; 2025) (Fig. 1).

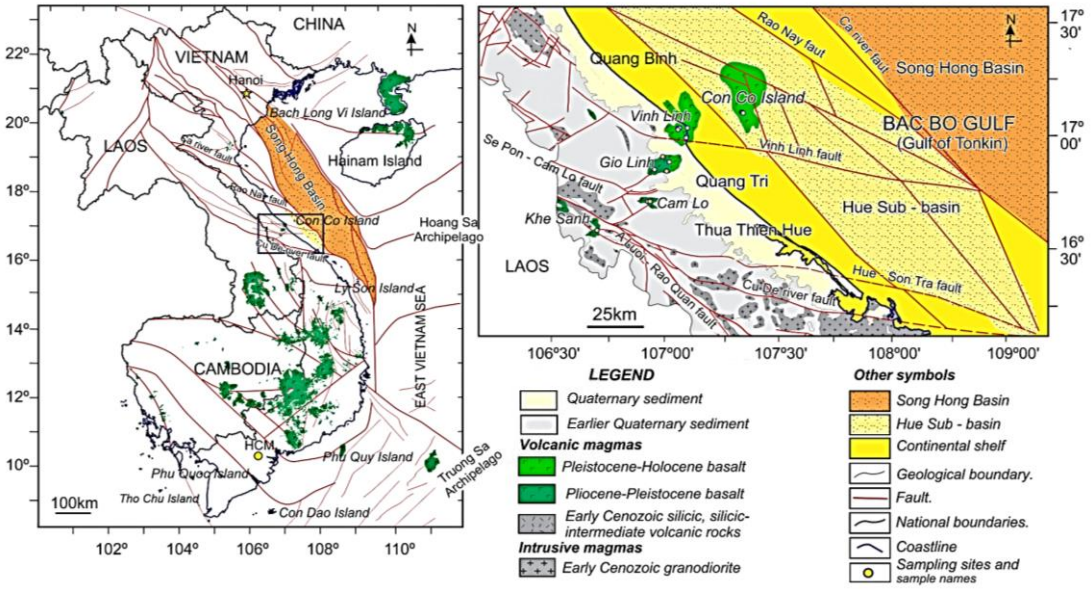

Figure 1. Scheme of regional structural map, showing major fault systems and the distribution of Mid Miocene-Holocene volcanics in Vietnam (left). The blow-up (right) illustrates the distribution of North Central Vietnam's monogenic volcanic fields, shown relative to the Hue-sub basin within The Red River Basin (simplified after Phan et al., 2012; Phung et al., 2023; Bui et al., 2023)

One of the most distinctive volcanic features is Con Co Island - a 2.3 km² cone-shaped island at the southeastern end of the RRSZ and within the Hue Sub-basin (HSB), a smaller structural unit along the western margin of the RRB. The HSB is believed to have formed due to the activity of the SCRNFS since the mid-Miocene. This fault system remains active and runs nearly parallel to other major fault systems in the north, including the RRSZ (Phung et al., 2023; Bui et al., 2023) (Fig. 1). Ar/Ar dating indicates

that the island formed around 0.35 ± 0.04 Ma (Lee et al., 1998). Geophysical studies have identified two distinct magmatic phases in this area: an early phase characterized by widespread lava flows and a later phase marked by localized cone-building activity under low-stress conditions (Tran et al., 2017; Phung et al., 2023).

Other notable basaltic fields include the Vinh Moc and Gio Linh volcanic areas along the coastal plain, and the Khe Sanh field further inland. The Vinh Moc and Gio Linh basalts vary in age from 1.5 to 1.0 million years (Ma), with new observations suggesting younger eruptive events (Cung et al., 1998; Lee et al., 1998; Hoang, 2023). The Khe Sanh field, dated to ~4.5 Ma, represents one of the earliest post-rift magmatic expressions inland (Fig. 1).

Overall, the monogenic volcanism in North Central Vietnam is characteristic of the diffuse igneous province spanning East and Southeast Asia (Tu et al., 1992; Hoang and Flower, 1998). Studies of Cenozoic basaltic volcanism across these areas indicate that the Indian Ocean mantle influenced the lead anomalies in their magmas, termed the DUPAL anomaly (Hart, 1984, 1988). The lead anomaly in East and Southeast Asia has been linked to west-directed asthenospheric flow and associated low-velocity zones that developed following the closure of the Neo-Tethyan Ocean due to the India-Eurasia collision (Tapponnier et al., 1982; Flower et al., 1998). This process likely played a critical role in generating thermally anomalous mantle domains beneath Indochina and the East Vietnam Sea (Zhang and Tanimoto, 1993; Zhu and Liu, 2025). These zones of elevated mantle temperature may have promoted partial melting, contributing to major regional tectonic events, including the opening of the EVS and the eastward rollback of the Pacific subduction system (Flower et al., 1998; Jolivet et al., 2018).

In addition to a generally hotter-than-average Asian mantle, other heat sources potentially contributing to mantle melting include: (1) a deep-seated, large-scale mantle plume (Yan et al., 2018; Hong-Anh et al., 2018); and (2) smaller-scale mantle upwellings or diapirs. Although current evidence does not support the presence of a primary deep-rooted heat source directly under North Central Vietnam, alternative melting mechanisms should be considered. In particular, decompression melting related to lithospheric stretching (Latin and White, 1990), in combination with the anomalously warm regional mantle (Hoang and Flower, 1998; Le et al., 2017; Yu et al., 2017; Zhu and Liu, 2025), likely played a crucial role in generating the observed volcanism.

This study investigates the origin and evolution of these intraplate volcanic systems by analyzing basaltic samples from Con Co Island, Vinh Moc, Gio Linh, and Khe Sanh. Petrographic, elemental, and isotopic data are used to infer mantle source properties, melting processes, and the role of lithospheric structures in magma generation.

2. Petrography, Sample preparation and Analytical procedures

2.1. Petrography

Basalt thin sections were prepared from fresh chunks for microscopic analysis. Basalts from Con Co Island are phyric subalkaline with subhedral to anhedral olivine being the only phenocryst. Plagioclase is a prism and needle-shaped mineral of various sizes. The groundmass consists of volcanic glass, plagioclase microlites, and Fe-Ti oxides. Basalts from Vinh Moc, a coastal area of Vinh Linh commune, are coarse-grained olivine and plagioclase-bearing phyric subalkaline to alkaline basalt, with intersertal texture on a needle-shaped plagioclase and rounded olivine microlite groundmass. The 4.5 Ma alkaline basalt from Khe Sanh is euhedral olivine phyric, set in a glass, plagioclase, and Fe-Ti oxide groundmass. Gio Linh subalkaline basalts are olivine-plagioclase phyric. The olivines are subhedral, partially

altered to chlorite and epidote; the plagioclases are elongated prisms or tabular; otherwise, fresh. The phenocrysts form clusters (aggregates) on volcanic glass, microlite, and amorphous groundmasses.

2.2. Sample preparation and Analytical procedures

The sample preparation for petrographic, geochemical, and isotopic analysis, including sample treatment to account for the effects of seawater interaction and secondary alteration, as well as loss-on-ignition, is described in Hoang et al. (2024; 2025) and is briefly outlined in the attached Supplementary files.

A set of samples from Gio Linh and the surrounding area was analyzed for K-Ar dating at the Far East Geological Institute (Vladivostok), using the procedure of Ignat'ev et al. (2010). The trace and minor element concentrations were acquired from a Neptune Elemental Q-ICP-MS at the University of the Ryukyus. Samples were analyzed three times; the values were averaged to calculate the standard deviations (±1σ).

The procedures for isotopic analysis are also described in Hoang et al. (2024, 2025); however, additional information is provided here.

A set of samples from Con Co Island and the Vinh Moc coastal area was acid-leached to eliminate possible seawater effects before the chemical chromatography. The strontium, neodymium, and lead isotopic data performed on unleached samples are usually different from those of leached and heated (baked) samples. The Sr and Pb are generally higher, and the Nd isotopic data are relatively lower compared with those of the leached and heated samples. The latter data are relatively similar and show good repeatability, accuracy, and standard deviation. Additionally, isotopic data acquired from the heated samples from a Neptune and a NU Plasma 3 MC-ICP-MS are almost identical. Therefore, this study reports only data acquired from heated samples.

The major, minor, and trace elements, as well as the isotopic compositions, along with age data, of North Central Vietnam's basalts are provided in the Supplementary files.

3. Analytical results

3.1. Major and minor element diagrams

Chemical data for the basalts from Vietnam's North Central region include samples from Con Co Island (0.36 Ma), Gio Linh (including Vinh Moc, Gio Linh, and Dong Ha: 0.56, 1.3, and 1.32 Ma), and Khe Sanh (4.5 Ma) (Fig. 1). Khe Sanh basalts are relatively low in SiO_2 concentrations (between 46 and 47 wt.%) and relatively high in Na_2O + K_2O = 4.2–5.2 wt.%, placing them in the alkaline basalt field (Fig. 2). In contrast, Con Co Island basalts show higher SiO_2 (50.3–52.3 wt.%) and high total alkaline oxides (4.4–5.2 wt.%), plotting within the subalkaline/tholeiitic basalt field (Fig. 2). Gio Linh basalts exhibit a narrow SiO_2 range (~51 wt.%) and total alkalis of 4.5–5.5 wt.%, straddling the boundary between the subalkaline and alkaline fields.

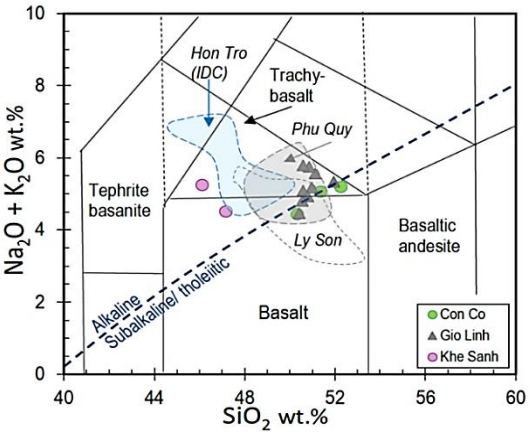

Figure 2. Plots of SiO_2 vs. Na_2O + K_2O (TAS) (after Le Bas et al., 1986) showing Vietnam's North Central basalts are mostly alkaline with a minor amount of sub-alkaline rock type. Data for the fields of Pleistocene-Holocene PQI, LSI, and IDC (Ile des Cendres) submarine volcanoes (IDC) are from Le et al. (2017), Hoang et al. (2021, 2025)

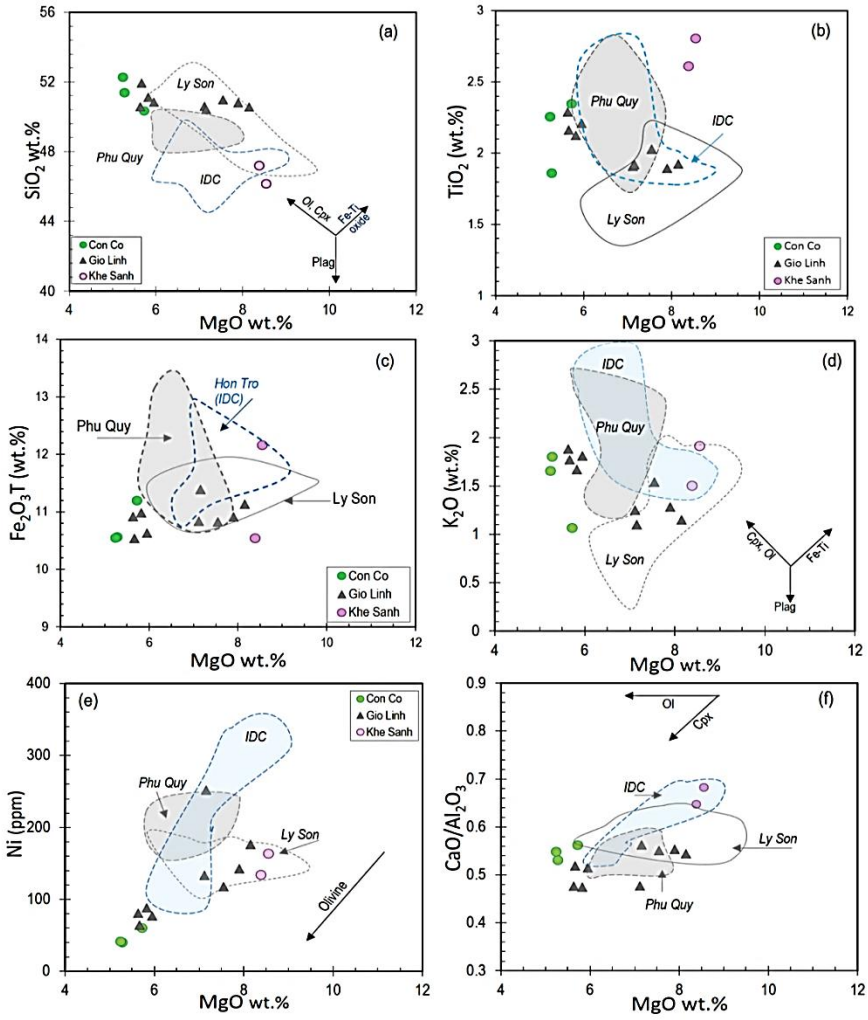

Figure 3. The correlation between (wt.%) MgO and SiO_2 (a), TiO_2 (b), Fe_2O_3T (c), K_2O (d), Ni (ppm) (e), and CaO/Al_2O_3 (f) is shown relative to Southeastern monogenic volcanoes at Phu Quy, Ly Son, and Ile des Cendres submarine. The data sources are as in Fig. 2. Arrows indicate evolving directions following mineral fractionation. The explanations are given in the text

MgO contents vary among the regions. Con Co Island basalts have the lowest MgO (~5.7 wt.%), whereas Gio Linh basalts range from 5.8 to 8.2 wt.%, and Khe Sanh basalts reach the highest MgO values (~8.5 wt.%). The latter also displays the lowest SiO_2, reinforcing their compositional distinction. A strong inverse correlation between SiO_2 and MgO (Fig. 3a) suggests significant olivine fractionation across the suite.

Khe Sanh basalts also contain the highest TiO_2 (up to 2.7 wt.%), although other basalts in the region show moderately high TiO_2 values (1.8–2.4 wt.%). Only Gio Linh basalts show a clear negative correlation between MgO and TiO_2, suggesting olivine fractionation. In contrast, the others exhibit no significant trend (Fig. 3b). The total iron, as $Fe_2O_3(t)$, is relatively high across the region (10.5–12 wt.%), with no correlation to MgO (Fig. 3c). K_2O concentrations are generally high (1–2 wt.%) and display scattered trends relative to MgO (Fig. 3d).

A generally linear correlation between Ni contents (ppm) and MgO further supports the fractionation of olivine and clinopyroxene in magma evolution (Fig. 3e). MgO versus CaO/Al_2O_3 plots, however, show distinct groupings within individual areas but appear scattered across regions, implying heterogeneous mantle sources or melting conditions (Fig. 3f).

For comparison, fields representing Pleistocene basalts from Phu Quy (PQI) and Ly Son (LSI) volcanic islands, as well as Ile des Cendres (IDC) submarine volcanoes in South Central and Southeastern offshore Vietnam, are shown (e.g., Le et al., 2017; Hoang et al., 2021, 2025). Most Gio Linh basalts fall outside these reference fields, although a few overlap with those of LSI and PQI (Figs. 2, 3a–f).

3.2. Trace element diagrams

The chondrite-normalized rare earth element (REE) configuration displays typical ocean island basalt (OIB)-like trends, with enriched light REEs (LREEs) smoothly decreasing toward heavy REEs (HREEs) (Fig. 4a). The La/Yb ratios for most samples range from 12 to 17, consistent with Miocene-Pleistocene subalkaline basalts elsewhere in Vietnam. An exception is the Khe Sanh alkaline basalt, which has a significantly elevated La/Yb ratio of 26.76. This is notably higher than the North Arch mantle plume-related basalts (~19.5; Frey et al., 2000) but comparable to average alkaline basalts from the Vietnam Western Highlands (~24; Hoang et al., 2019).

Trace element patterns normalized to primitive mantle also exhibit OIB-like signatures, with general enrichment of incompatible elements (Fig. 4b). Minor anomalies are observed in the high-La/Yb Khe Sanh sample, including relatively high Nb, Ta, and Sr, and low U and Th, possibly reflecting source heterogeneity or secondary alteration effects.

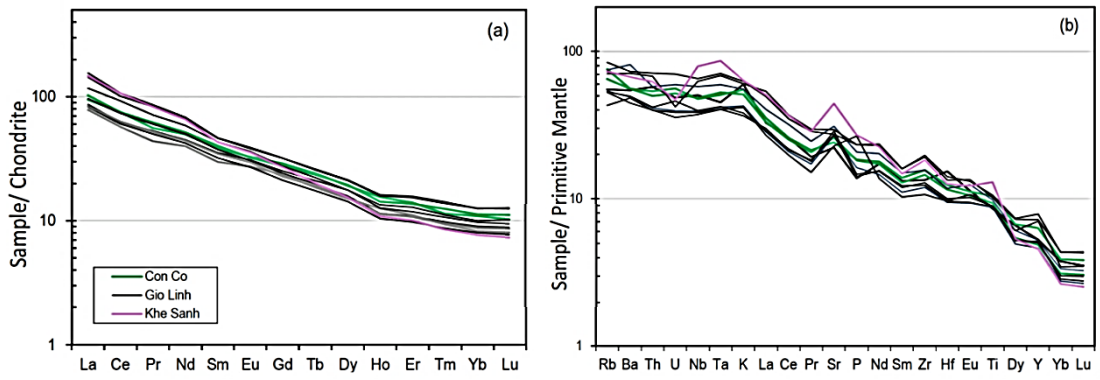

Figure 4. Chondrite rare earth element normalization patterns (a) and primitive mantle trace element normalized configuration (b) of the North Central recent basalts. Normalizing data is after McDonough and Sun (1995). The gentle decrease from light rare earth (LREE) to heavy REE character suggests an OIB-type

3.3. Sr, Nd, Hf, and Pb isotope characteristics

3.3.1. The correlation between $^{87}Sr/^{86}Sr$ and $^{143}Nd/^{144}Nd$

The $^{87}Sr/^{86}Sr$ values of the studied basalts range between 0.7040 (Khe Sanh) and 0.7046–0.7050 (Con Co and Gio Linh), accompanied by corresponding $^{143}Nd/^{144}Nd$ values expressed as εNd from 3.8 (Khe Sanh) to 0.9–2.2 (Con Co and Gio Linh). These data plot within the depleted mantle quadrant (Fig. 5). Con Co and Gio Linh basalts, with higher $^{87}Sr/^{86}Sr$ and lower εNd, overlap

isotopically with the relatively enriched fields of the PQI and IDC in Vietnam's South Central offshore region, while remaining isotopically distinct from the more enriched LSI basalts (Le et al., 2017; Hoang et al., 2021; 2025). Meanwhile, the Khe Sanh Pliocene alkaline basalts plot firmly within the depleted OIB-like field. These isotopic variations highlight the spatial and temporal heterogeneity of Sr and Nd isotopic compositions in the North Central volcanic rocks of Vietnam (Fig. 5).

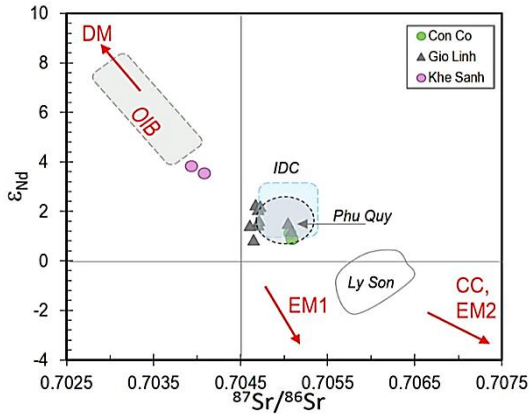

Figure 5. Plots of $^{87}Sr/^{86}Sr$ vs. ε_{Nd} for the North Central Vietnam basalts, plotted relative to major mantle isotope components, such as DM: depleted mantle; EM1 and EM2: enriched mantle type 1 and 2; CC: continental crust. Data sources for PQI, LSI, and IDC are as in Fig. 2. See the explanation in the text

3.1.2. The correlation between $^{206}Pb/^{204}Pb$ and $^{207}Pb/^{204}Pb$ and $^{208}Pb/^{204}Pb$ isotopic ratios

The lead isotope compositions of Khe Sanh, Con Co, and Gio Linh basalts are relatively radiogenic. For instance, $^{206}Pb/^{204}Pb$ values vary between 18.7 and 18.8, $^{207}Pb/^{204}Pb$ range from 15.60 to 15.73, while $^{208}Pb/^{204}Pb$ values vary between 38.9 and 39.65. Khe Sanh samples exhibit the lowest Pb isotopic ratios, while Con Co Island basalts have the highest (Figs. 6a-b). Despite Con Co and Gio Linh samples overlapping with the PQI and IDC fields in Sr-Nd isotope space, their Pb isotopes more closely resemble those of LSI, trending toward a continental crust (CC) or enriched mantle type 2 (EM2) signature. In contrast, basalts from PQI and IDC plot above the Northern Hemisphere Reference Line (NHRL) and the Pacific MORB (P-MORB) (White et al., 1987), aligning more with Indian (I-) MORB fields characterized by lower $^{206}Pb/^{204}Pb$ relatively higher $^{207}Pb/^{204}Pb$ and $^{208}Pb/^{204}Pb$ (Holm, 2002; Mahoney et al., 2002).

In summary, North Central and Ly Son basalts trend toward CC or EM2 sources, whereas basalts from the southeastern offshore regions show greater affinity with EM1-like sources (Figs. 6a-b).

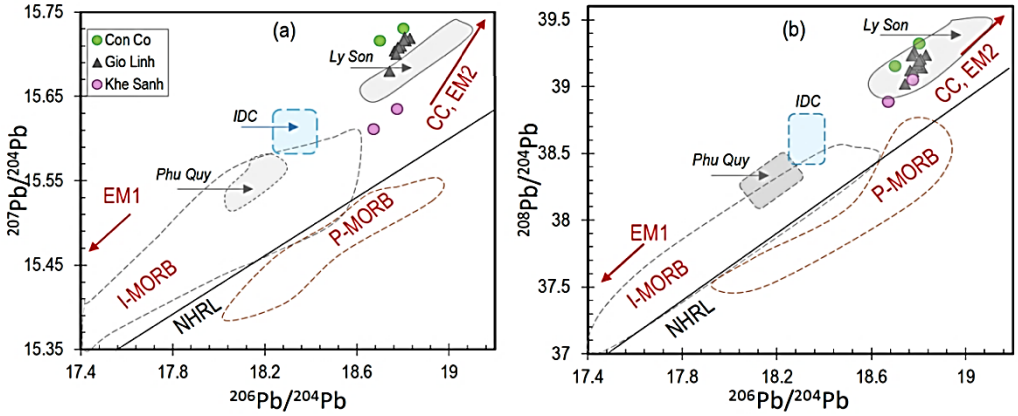

Figure 6. Plots of $^{206}Pb/^{204}Pb$ vs. $^{207}Pb/^{204}Pb$ (a) and $^{208}Pb/^{204}Pb$ (b) for the North Central Vietnam basalts. Data sources for Indian Mid-Ocean Ridge basalt (I-MORB) are from Holm (2002) and Mahoney et al. (2002); data for Pacific MORB are from White et al. (1987). NHRL: Northern Hemisphere Reference Line is after Hart (1988). Other data sources are as in Fig. 2. See the explanation in the text

3.1.3. $^{206}Pb/^{204}Pb$ vs. $^{87}Sr/^{86}Sr$ diagram

When plotted together with monogenetic volcanoes in South Central and Southeastern offshore Vietnam (e.g., LSI, PQI, and IDC), the North Central basalts form a distinct isotopic field (Fig. 7). They display varying $^{87}Sr/^{86}Sr$ and $^{206}Pb/^{204}Pb$ values and do not overlap with any of the offshore volcanic fields. This distribution indicates that both the North Central and monogenetic basalts were influenced by at least three isotopic endmembers: a depleted mantle (DM), EM1, and EM2, consistent with the mantle component model proposed by Hoang et al. (2025).

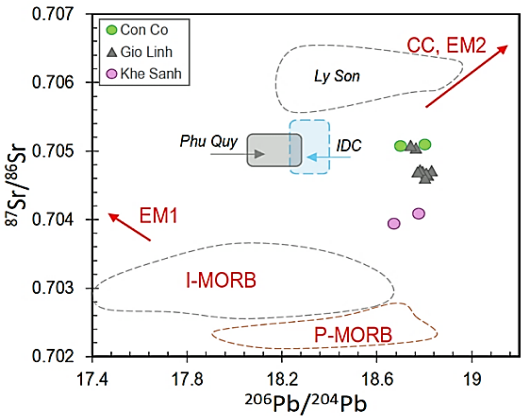

Figure 7. Plots of $^{87}Sr/^{86}Sr$ vs. $^{206}Pb/^{204}Pb$ for the North Central Vietnam basalts show that each of the volcanic centers is distributed separately. Data sources for reference fields are as in Figs. 5 and 6

3.1.4. ε_{Nd} vs. ε_{Hf}

The εNd versus εHf diagram includes isotopic data from North Central Vietnam basalts, along with reference fields from South Central Vietnam (Richard et al., 2024), the southeastern RRSZ (Hoang et al., 2024), and the EVS (Fig. 8). These data plot along the terrestrial array and are referenced against major mantle reservoirs, including depleted mantle (DM), enriched mantle (EM), OIB, and MORB sources (e.g., Jones et al., 2019). North Central basalts exhibit εNd and εHf values slightly more radiogenic than CHUR (chondritic uniform reservoir), yet more enriched than those of the South Central, EVS-MORB, and SE RRSZ basalts. They trend toward the EM field, reflecting a significant contribution from enriched mantle components (Fig. 8).

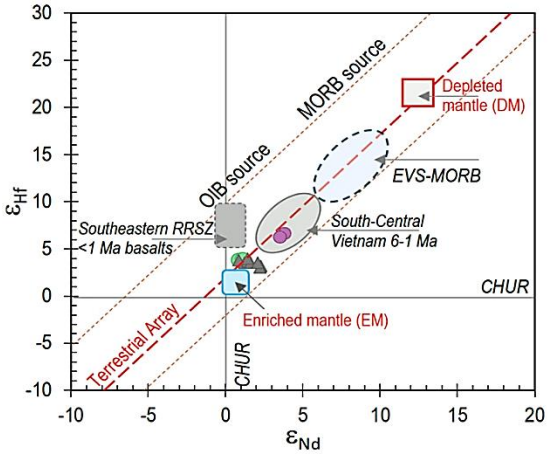

Figure 8. Plots of $^{176}Hf/^{177}Hf$ versus $^{143}Nd/^{144}Nd$ (expressed as ε_{Hf} versus ε_{Nd}) for the North Central Vietnam basalt relative to the main mantle isotopic components and chondrite uniform reservoir (CHUR) (modified from Jones et al., 2019). The data field for the East Vietnam Sea (EVS-MORB) is from Hoang et al. (2025), South Central Vietnam is from Richard et al. (2024), and the Southeastern Red River Shear Zone (RRSZ) is from Hoang et al. (2024)

4. Discussions

4.1. Crustal contamination: evidence and evaluation

The North Central Vietnam basalts exhibit relatively high strontium and lead isotopic ratios, alongside low neodymium isotopic values. At first glance, this isotopic signature may suggest crustal contamination, as such patterns are typically associated with the incorporation of continental material. Crustal contamination often results in elevated concentrations of highly incompatible elements, including Ba, Sr, and Th, and a depletion in (for example) Zr, Nb, and Ta. Consequently, contaminated magmas

typically display elevated Ba/Zr, Ba/Nb, or Th/Nb ratios, which show a positive correlation with Sr and Pb and a negative correlation with Nd isotopic ratios (Tatsumi, 1989; McLennan, 2001).

However, the geochemical patterns in the North Central basalts do not support this hypothesis. The $^{87}Sr/^{86}Sr$ ratios show no consistent correlation with Th/Nb (Fig. 9a). Instead, basalts from different volcanic fields occupy distinct compositional fields, suggesting geochemical isolation and limited interaction with crustal materials (Rudnick and Fountain, 1995).

Moreover, a positive correlation between Th and Nb is observed, with Th/Nb values ranging between 0.09 and 0.13 comparable with the primitive mantle at 0.12 (Hofmann, 1988), but are much lower than the Upper Continental Crust (UCC) with the average Th/Nb ratio 3.75 (Taylor and McLennan, 1981) (Fig. 9b). Additional evidence is provided by the correlation diagram between Ce/Pb and Ce (Fig. 10), where North Central basalts plot within the mantle-derived field and above the subduction-related and upper continental crust domains (Kimura and Yoshida, 2006; McLennan, 2001).

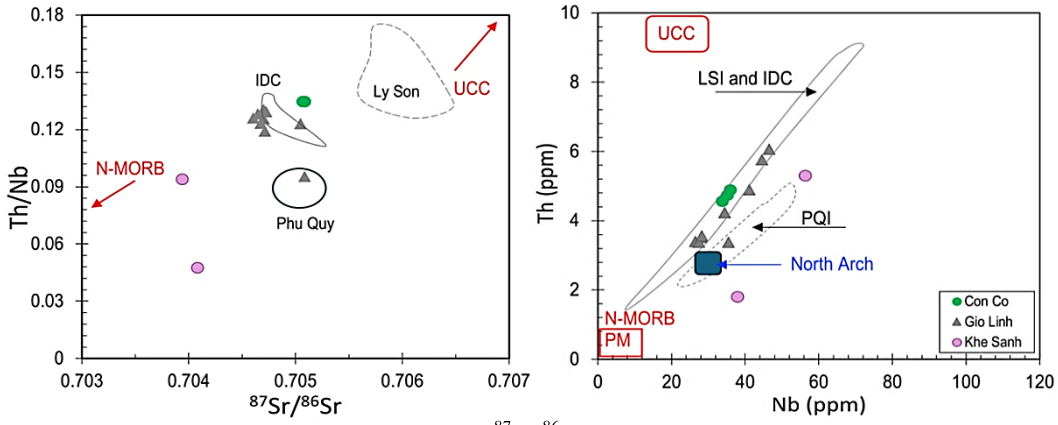

Figure 9. The correlation between Th/Nb and $^{87}Sr/^{86}Sr$ (a) and between Th and Nb (b) for the North Central Vietnam basalts is vastly vertical, suggesting a minor crustal effect. The basalts' average Th/Nb ratio is about 0.11, roughly about the MORB, PM values (0.07-0.08), and hotspot-derived North Arch basalts (Frey et al., 2000) much smaller than that of continental crust (CC) upper continental crust (UCC) at 0.43 (after Taylor and McLennan, 1981; Rudnick and Fountain 1995) and NE Japan arc at 0.66 (Kimura and Yoshida, 2006). The data sources for PQI, LSI, and IDC basalts are presented in Fig. 2.

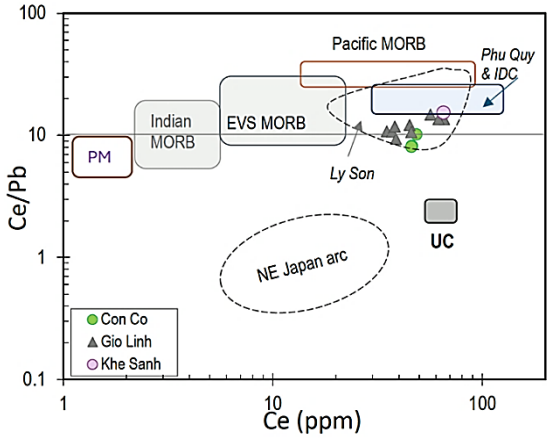

←*Figure 10*. Plots of Ce (ppm) versus Ce/Pb for the North Central Vietnam basalts are plotted relative to several prominent geochemical representatives, such as PM (primitive mantle: McDonough and Sun, 1995), Indian MORB (Neal et al., 2002), EVS-MORB, Pacific MORB (Regelous et al., 1999), NE Japan Arc (Kimura and Yoshida, 2006), Upper crust (Rudnick and Fountain, 1995). Data sources for PQI, LSI, and IDC are given in Fig. 2. See the detailed explanation in the text

Since Th is enriched in crustal and hydrous fluid-related environments, and Nb is believed

to be retained in residual phases and depleted in crustal material, their equally high concentrations in these basalts suggest a mantle origin. The comparable enrichment of both Th and Nb is more conforming to partial melting of a heterogeneous mantle source than to crustal assimilation (Gill, 1981; Tatsumi, 1989; McLennan, 2001).

In summary, the elemental ratios and highly enriched isotopic characteristics indicate that the North Central Vietnam basalts were derived from the mantle and remained largely unaffected by crustal contamination during their ascent.

4.2. Melting depths of the North Central Vietnam basalts

Understanding the conditions under which the North Central Vietnam basalts were generated requires estimating the pressure and temperature of partial melting, which relies on reconstructing the *composition of the primary melts*. These melts have typically experienced varying degrees of fractional crystallization before eruption, as indicated by phenocrysts beyond olivine.

Most samples in this study have MgO contents (wt.%) varying from 5.5 to 7.0, except for two Khe Sanh samples that exceed 8.0 wt.%. Corresponding Mg# values range from 51 to 62.5, which are consistent with equilibrium crystallization of olivine forsterites with Fo78–Fo84.8, based on an Fe/Mg partition coefficient between olivine and liquid at 0.30 (e.g., Roeder and Emslie, 1970). EPMA analysis on olivine phenocrysts in North Central Vietnam's basalts reveals core compositions of Fo78–Fo82 and rim compositions down to Fo55–Fo70 (Nguyen Hoang, unpublished), suggesting progressive olivine and clinopyroxene (±plagioclase) fractionation. Assuming a mantle olivine composition up to Fo90, the forsteritic compositions indicate moderate to extensive olivine fractionation (Yamashita and Tatsumi, 1994; Putirka, 2008).

Two different approaches were applied to reconstruct the *primary melt compositions*, for samples with MgO ≥ 8 wt.% and whole-rock/olivine equilibrium Fe/Mg partition coefficients < 0.30 ± 0.03, the Putirka (2008) method was used. In this method, equilibrium olivine was added to the melt until the melt's MgO concentration increased to 13–16 wt.% and forsterite content peaked at Fo89–Fo90. For evolved samples, with MgO lower than 8 wt.%, and whole-rock and clinopyroxene phenocrysts exhibiting equilibrium distribution coefficients greater than 0.27 ± 0.03, the Danyushevsky and Plechov (2011) method was applied. This method involved adjusting the proportions of olivine and clinopyroxene until the melt reached ~8 wt.% MgO, followed by further correction after Putirka (2008). The *computed melt compositions* are summarized (Supplementary files) and explained in Figures 11, 12, and 14.

The FeO and SiO_2 compositions of the *calculated primitive melts* were then applied to infer melting temperatures and pressures, respectively (Table 2 in Supplementary files). Subalkaline basalts from Con Co and Gio Linh fall within the 15 kbar melting range, based on HK66 melting experiments (e.g., Hirose and Kushiro, 1993). Whereas an older Khe Sanh alkaline basalt (4.5 Ma) exhibits a melting pressure of 29 kb, indicating deeper melting. Regardless of the difference in the melting pressures, their range of melting temperatures is narrow, just from 1360 to 1400°C (Fig. 11a-b). Overall, the inferred melting depths for North Central Vietnam basalts are shallower than those estimated for monogenic volcanic centers in South Central and Southeastern offshore Vietnam (Hoang et al., 2025).

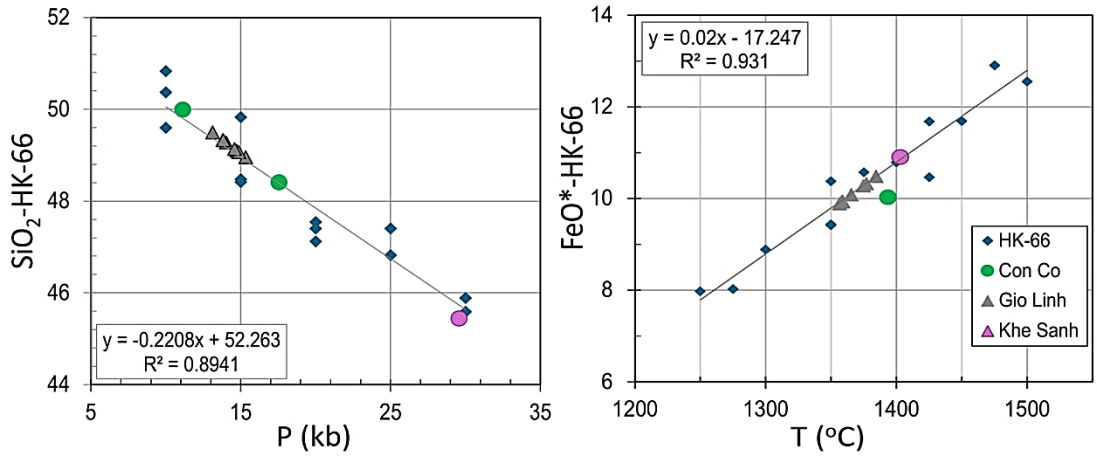

Figure 11. Plots of (a) SiO_2 and (b) FeO for *computed primitive melts* of the North Central Vietnam basalts are plotted against the experimental pressures and temperatures of HK-66 spinel-lherzolite melts (Hirose and Kushiro, 1993). Except for a Khe Sanh and a Con Co alkaline basalt in the 29 kb field, the remaining basalts are roughly distributed in the 15 kb field, with a Khe Sanh basalt showing the highest melting temperature at 1403°C. Data for *computed primitive melts* of PQI and LSI, as well as IDC basalts, are illustrated for reference; their data sources are as shown in Fig. 2

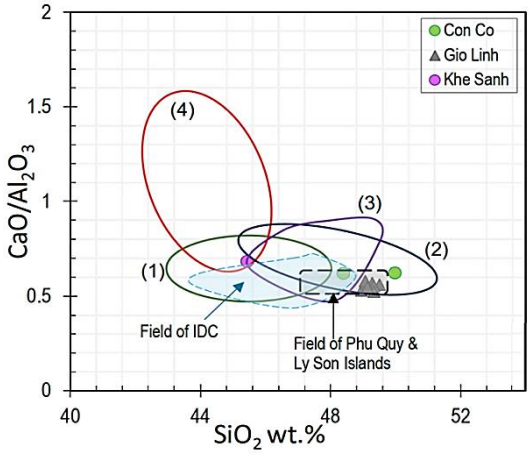

Figure 12. Correlation between SiO_2 (wt.%) and CaO/Al_2O_3 of *computed primitive melts* for the North Central Vietnam basalts is seen relative to compositional fields of experimental melting peridotite sources: (1) spinel peridotite (Gaetani and Grove, 1998), (2) spinel peridotite (Hirose and Kushiro, 1993), (3) garnet peridotite (Kushiro, 1998), and (4) garnet peridotite (Herzberg and Zhang, 1996; Tenner et al., 2012). Redrawn with modification from Liu et al. (2014). Also plotted are fields of PQI and LSI, as well as IDC computed primitive melts, for comparison. A detailed explanation is given in the text.

Generally, the *computed primitive melts* and supporting xenolith data indicate that the North Central Vietnam basalts were generated at relatively lower temperature and pressure conditions in the upper mantle, primarily in the presence of spinel peridotite.

4.3. Enrichment of the mantle source

The characteristics of rare earth and trace elements were analyzed and interpreted to examine the level of source enrichment in the mantle of North Central Vietnam. Davidson et al. (2013) proposed using the Dy/Dy* ratio to evaluate REE curve profiles, offering a means to differentiate magmatic evolution and source variations. Their study revealed that LREE-depleted arc magmas, such as those from the Tonga-Kermadec region, have higher Dy/Dy* values and concave-down REE patterns. In contrast, LREE-enriched magmas (e.g., Philippines, Indonesia) display lower Dy/Dy* and concave-up patterns. Within single volcanic systems, a decrease in Dy/Dy* and Dy/Yb often results from amphibole fractionation. Importantly, MORB, OIB, and

arc data collectively point to variably enriched MORB-like mantle sources, with high Dy/Yb values in OIB suggesting a role for garnet-bearing lithologies in their genesis.

In Fig. 13, most North Central Vietnam basalts plot to the left of the OIB field, overlapping with Ly Son Island basalts, implying similar mantle enrichment characteristics. However, one older Khe Sanh sample (4.5 Ma) and a Gio Linh sample (1.3 Ma) exhibit higher Dy/Yb values than the others and plot separately, suggesting a substantial garnet influence, comparable to that of PQI and IDC submarine basalts. These outliers may reflect melts derived from greater depths or garnet-bearing mantle sources.

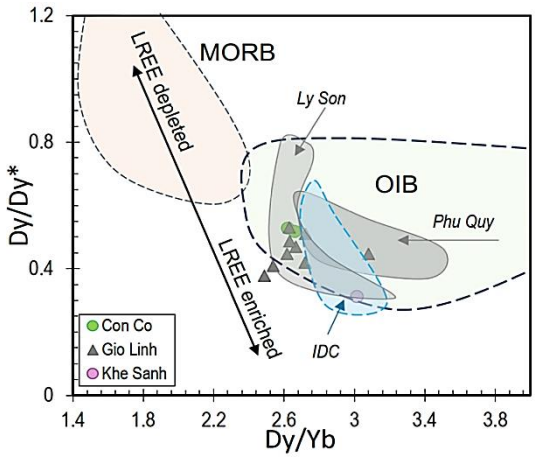

Figure 13. Plots of Dy/Dy* vs. Dy/Yb (e.g., Davidson et al., 2013) showing directions of light rare earth element enrichment (OIB) and depletion (MORB) relative to their mantle-derived sources. North Central Vietnam basalts plot in the OIB field with various degrees of garnet-bearing influences

High P-T petrologic experiments by Hirose and Kushiro (1993) show that melting relatively fertile peridotites (HK-66 and KLB-1) under a wide range of conditions typically contain TiO_2 less than 1.6 wt.% and K_2O less than 1.1 wt.%. However, experiments performed by Hirschmann et al. (2003) demonstrated that melts of mantle garnet pyroxenite can produce significantly higher TiO_2 contents, up to 2.5 wt.% at 25 kb and 1455°C. *Computed primitive melt compositions* for the North Central and Southeastern offshore monogenic basalts (Le et al., 2017; Hoang et al., 2024; 2025; this study) consistently show higher TiO_2 and K_2O than expected from peridotite melting alone (Fig. 14). This suggests an additional contribution from an enriched, non-peridotitic component.

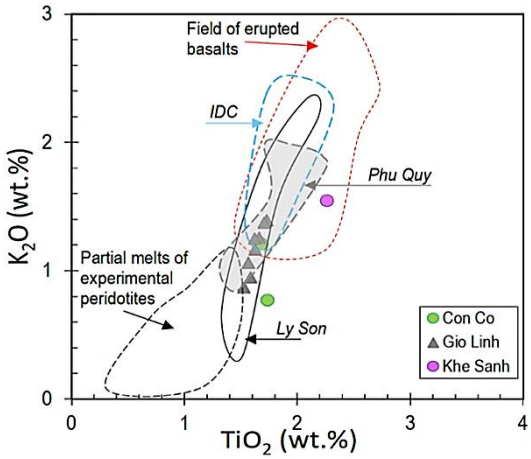

Figure 14. Plots of K_2O vs. TiO_2 contents for North Central basalts' *computed primitive melts* compared to experimentally peridotite melts (e.g., Hirose and Kushiro, 1993; Kushiro, 1996; 1998) and actual erupted basalts (red dashed line). The field of computed primitive melts of Ly Son, Phu Quy, and Ile des Cendres basalts is shown for reference (data from Hoang et al., 2021; 2025)

Prytulak and Elliott (2007) similarly argued that peridotite melting alone cannot explain high-Ti OIB compositions. Instead, they proposed minor contributions. 1–10% the melting of the recycled oceanic crust can reconcile the observed isotopic and trace element signatures. Such enriched melts likely form at greater depths than ambient peridotite, especially beneath thick lithosphere. However, the recycled crust alone may not fully account for the isotopic diversity in intraplate basalts; additional components, such as subducted sediments or

metasomatic veins, may also be involved (McKenzie et al., 2004; Prytulak and Elliott, 2007).

In conclusion, the North Central Vietnam basalts exhibit radiogenic isotopic signatures, elevated TiO_2 and K_2O contents, and enrichments in incompatible and high-field strength elements. These features and their inferred melting conditions indicate derivation from a fertile, enriched spinel peridotite asthenospheric source, likely modified by contributions from Ti-rich recycled oceanic crust or other enriched mantle lithologies.

Prytulak and Elliott (2007) similarly argued that peridotite melting alone cannot explain high-Ti OIB compositions. Instead, they proposed minor contributions. 1–10% of recycled oceanic crust melts can reconcile the observed isotopic and trace element signatures. Such enriched melts likely form at greater depths than ambient peridotite, especially beneath thick lithosphere. However, the recycled crust alone may not fully account for the isotopic diversity in intraplate basalts; additional components, such as subducted sediments or metasomatic veins, may also be involved (McKenzie et al., 2004; Prytulak and Elliott, 2007).

In conclusion, the North Central Vietnam basalts exhibit radiogenic isotopic signatures, elevated TiO_2 and K_2O contents, and enrichments in incompatible and high-field strength elements. These features and their inferred melting conditions indicate derivation from a fertile, enriched spinel peridotite asthenospheric source, likely modified by contributions from Ti-rich recycled oceanic crust or other enriched mantle lithologies.

4.4. Regional geodynamics

The regional geodynamic evolution of North Central Vietnam is intimately linked to lithospheric deformation, fault-controlled basin development, and deep mantle dynamics. During the Oligocene-Early Miocene, the RRB formed as a pull-apart basin on a thinned, northwest-southeast-trending lithosphere. Stratigraphic and structural evidence, such as rift-related unconformities, symmetric normal faulting, and a shift from continental to shallow marine deposition, indicates a phase of pure shear extension, followed by post-rifting thermal subsidence (Phan et al., 2012; Bui et al., 2023).

During the Middle to Late Miocene, a reorganization of the regional stress field led to a decline in left-lateral strike-slip motion along the RRSZ (Phan et al., 2012), accompanied by the emergence of right-lateral faulting and tectonic inversion along the western basin margin (Rangin et al., 1995).

On the RRB's southwestern margin, the Hue Sub-basin (HSB) evolved in connection with the SCRNFS, a right-lateral normal fault that extends offshore. Although the total offset along the SCRNFS is modest compared to the RRSZ, localized rifting driven by this right lateral shearing likely triggered a pull-apart opening of the HSB in the Late Oligocene-Middle Miocene (Bui et al., 2023; Phung et al., 2023).

Nguyen et al. (2018) proposed a regional gravity model that suggested notable depth modification in the crust-mantle boundary (Moho) across the SSB, particularly in the Quang Tri and Hue areas. Along the continental margin, the Moho lies at depths of 29–30 km, but it rises sharply to 24–25 km beneath the coastal areas of Quang Tri and Hue and continues to shallow towards the continental shelf, where it reaches depths of 20–22 km. This pattern indicates typical crustal thinning, characteristic of stretched continental margins, likely resulting from rifting-related tectonic activity and/or mantle upwelling leading to thermal erosion in the lower crust. These data suggest a coupling between deep mantle flow and crustal deformation in North Central Vietnam (Nguyen et al., 2014, 2018).

4.5. Melting mechanism for the North Central magmatism

Geochemical studies of Cenozoic basalts from Southeast and East Asia show an Indian Ocean mantle influence characterized by the DUPAL anomaly (Hart, 1984; 1988), interpreted as attributed to east-directed asthenospheric flows from the Neo-Tethyan mantle following its closure due to the collision between India and Eurasian plate in the Tertiary (Flower et al., 1998, 2001). These mantle dynamics, especially, are essential in shaping the post-collisional evolution of East and Southeast Asia. Recently, more geochemical, geophysical, and structural models have supported the presence of two distinct mantle flow regimes with contrasting depths and directions under the Eurasian mantle. A deeper mantle current (> 200 km), flowing from the Indian Ocean toward the Northeast, likely established the regional stress field during the early Miocene. Concurrently, a shallower mantle flow (~100 km depth) characterized by a high potential temperature (~1400°C) was likely driven by vortex-like motions related to peripheral subduction and edge-driven tectonic anomalies (Jolivet et al., 2018).

Zhu and Liu (2025) recently compiled an extensive dataset of heat flow measurements across the EVS region. Their study revealed the terrain is characterized by a high-thermal regime, with an average surface heat flow of ~75 mW/m² and lithospheric thicknesses ranging from 60 to 80 km. A thinner lithosphere is found beneath the central basin, while a thicker lithosphere underlies the continental margins. They attributed this elevated heat flow primarily to mantle upwelling, consistent with the region's active rifting and recent volcanic activity (Zhu and Liu, 2025).

Further insights into the thermal structure of the region are provided by seismic tomography. Yu et al. (2017) used S-wave velocity-temperature relationships to find that mantle temperatures beneath Southeast Asian rift zones are ~200°C higher than those beneath stable plateaus (e.g., Khorat, Bolaven) and subduction zones. Earlier, Hoang and Flower (1998) had estimated mantle Tp beneath Indochina and the southeastern EVS to be 100–150°C above the global average (i.e., reaching 1380–1430°C). Yu et al. (2017) provided more specific estimates, suggesting Tp values of 1400–1500°C beneath the western EVS (near the Paracel Islands) and 1550–1600°C beneath southeastern Vietnam at depths of 100–120 km. They proposed a regional geotherm with Tp ~1400°C as appropriate for the tectonic setting.

As no direct data on lithospheric thickness in the North Central region is available, we adopt a proxy value of 80 km based on the thickest lithosphere along the regional continental margin (Zhu and Liu, 2025). Regional average heat flow values are taken from Nguyen et al. (2014), who reported a range of 65–75 mW/m² for the RRB. A simple boundary layer melting model (e.g., Latin and White, 1990; Anderson, 1995) is employed, using these assumptions and values from the literature.

Mayle and Harry (2023) studied models of rift-related melting, suggesting that mafic components in the base of the lithosphere and at the top of the asthenosphere start to melt at a small extension rate, 0–35% or (extension factor) β = 1–1.2, but reaching larger melt production between 0–65% extension (equivalent to β = 1–1.5). They assumed that if hydrous peridotite is present, it can begin melting as soon as the onset of extension, with maximum melting taking place at up to 180% extension (β = 3). However, like Harry and Leeman (1995), they suggested this early melting phase would soon dehydrate the mantle, shifting the melting regime toward that of dry peridotite (Mayle and Harry, 2023).

To explain the recent occurrence of monogenic volcanism in North Central Vietnam, we present a model in which the lithospheric mechanical boundary layer (MBL) consists of a refractory, isotopically heterogeneous mantle lying below the crust (Turner and Hawkesworth, 1995; Anderson, 1995). Beneath the MBL is the thermal boundary layer (TBL), characterized by reduced shear-wave and low velocity zones marking the transition from conductive to convective heat transfer. It coincides with the inflection point of the thermal gradient closest to the peridotite solidus, where melt generation is most likely, and is inferred to be enriched and fertile (Hoang and Flower, 1998). The underlying asthenosphere is typically isotopically depleted, unless modified by recycled subducted lithospheric sediments introduced via plume activity or delamination (Prytulak and Elliot, 2007; Castillo, 2018) and is residual to early crustal extraction (Hofmann, 1988).

The depth and amount of mantle melting are mainly controlled by two factors: the temperature of the mantle (Tp) and the amount of H_2O in the mantle rocks. These factors determine when the rock starts to melt, and their effects are shown in Fig. 15. The figure also includes a temperature profile (adiabat) of the mantle beneath North Central Vietnam, compiled using the *computed primitive melt* compositions.

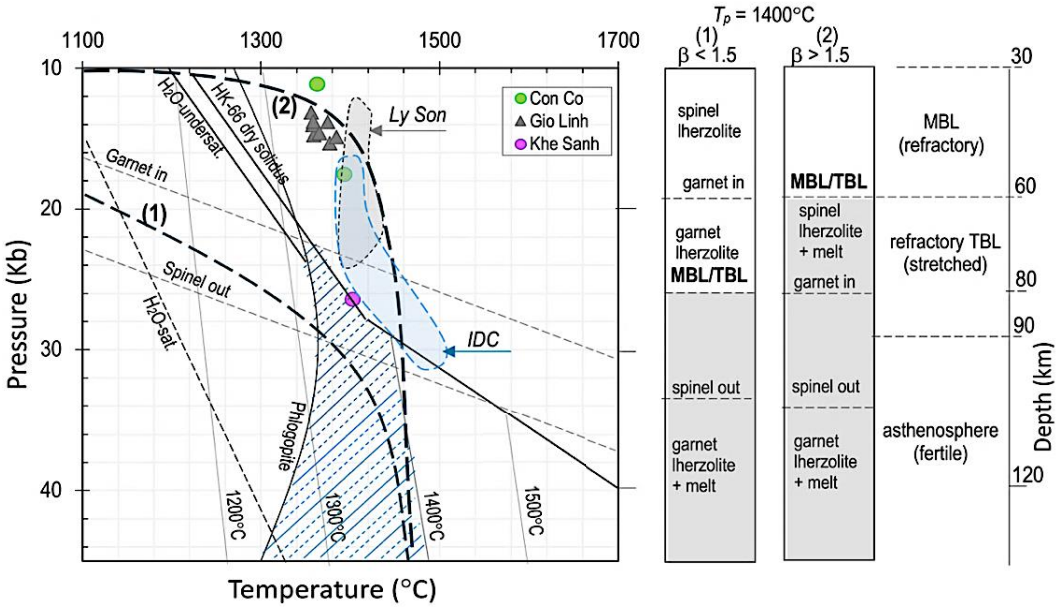

Figure 15. An illustration of the asthenosphere-lithosphere boundary shows the fertile peridotite solidus of HK-66 (Hirose and Kushiro, 1993), stability fields of phlogopite (Modreski and Boetcher, 1973), The spinel-garnet transition, and an H_2O-undersaturated solidus (simplified from Hoang and Flower, 1998). Melt segregation conditions for the computed primitive melt compositions of North Central Vietnam indicate an asthenospheric potential temperature (Tp) of ~1400°C. The shaded region marks the P–T field for incipient H_2O-saturated melting. At Tp = 1400°C and β ≈ 1.0, conductive heat flow is ~75 mW/m², producing Type 1 lithospheric geotherms. Type 2 adiabatic geotherms form from uniform stretching at β ≈ β 1.5 to 2, with a heat flow of up to 130 mW/m², causing melting at depths of ~45–60 km. The data sources for the fields of LSI and IDC are as shown in Fig. 2. Detailed explanations are provided in the text

One key process is the breakdown of phlogopite, which typically occurs at a depth of approximately 110 km under normal Tp conditions. However, if the mantle is hotter than usual, above 1400°C, this breakdown occurs at shallower depth, typically less than 90 km (McKenzie and Bickle, 1988; Wilson, 1993; Hoang and Flower, 1998). In North Central Vietnam, the estimated mantle temperature is approximately 1400°C, which is hotter than the average beneath most continents, indicating that the lithospheric mantle here is relatively thin, at around 80 km (Yu et al., 2017; Zhu and Liu, 2025).

In regions where the lithosphere is not being stretched significantly (low β), heat moves primarily by conduction, forming the Type-1 geotherm (Fig. 15). This type of thermal structure has been observed through mantle xenolith thermobarometry in similar settings (Ionov et al., 1998). However, if the lithosphere is stretched to a larger extent (with thinning of 20 to 40 km), the heat flow changes, leading to a Type-2 geotherm. This type typically occurs when the stretching factor (β) is between 1.5 and 2, as shown in the thermal model in Fig. 15 (Latin and White, 1990; Anderson, 1994; Hoang and Flower, 1998; Mayle and Harry, 2023).

As shown in Fig. 15, when the lithosphere stretches, the lithospheric mantle layer beneath the crust (MBL) becomes a weaker and more variable layer, known as the Thermal Boundary Layer (TBL). This transformation causes the depth at which the melting starts to become shallower, shifting the boundary where water is released from minerals upward. As the stretching continues, the pressure drops, and some parts of the mantle begin to melt, particularly in peridotites that contain both garnet and spinel. As the melt rises, it may react with surrounding rocks below the melting point, which helps explain why the resulting North Central Vietnam basalt compositions are diverse. Importantly, this model avoids requiring melting to happen in the strong MBL, which solves a problem: the melts we observe seem to form at pressures below 15 kb, but the lithosphere is thicker than 80 km, which should produce higher pressures.

Additional evidence for a hot environment below the surface includes a shallow crust-mantle boundary (only 20–22 km) beneath the North Central continental shelf and very high heat flow, up to 130 mW/m^2, much higher than the 65–75 mW/m^2 recorded in the nearby Red River Basin (Nguyen et al., 2014; 2018, 2022; Pham et al., 2019).

5. Conclusions

(1) Small-scale monogenic subalkaline and tholeiite basalt volcanism, dating from Pliocene to Pleistocene, is widespread in North Central Vietnam, including 0.35 Ma sub-alkaline/tholeiite at Con Co Island, 1.5 to 1.3 Ma sub-alkaline to alkaline basalt in the Gio Linh area (including Vinh Moc and Dong Ha), and 4.5 Ma alkaline basalt from Khe Sanh. Situated within the southeastern tip of the Red River Shear Zone, these volcanoes appear to be linked to pull-apart rifting of the Hue Sub-basin associated with the Song Ca-Rao Nay Fault System.

(2) The petrogenetic conditions of parental magmas were interpolated for (computed) primitive compositions from experimental studies, and suggest they segregated from their mantle source temperature of 1350 to 1400°C and pressures of 15 to 29 kb, consistent with decompression melting of a spinel peridotite source.

(3) The basalts exhibit oceanic island basalt (OIB)-type geochemistry, characterized by enrichment in Sr, Nd, Hf, and Pb radiogenic isotopes, large ion lithophile elements (LILE), high field strength elements (HFSE), and ligh rare earth elements, consistent with variable metasomatic enrichment of a fertile asthenosphere source.

(4) The North Central Vietnam volcanism is part of an east and southeast Asian 'diffuse igneous province' characterized by anomalous, DUPAL-type mantle. This isotopic anomaly has been attributed to the assimilation (via delamination) of ancient EM1-rich cratonic lithosphere during east- and southeast-directed asthenospheric flow induced by the early Tertiary India-Eurasia collision.

(5) Interestingly, while the geochemical data provide insights into the mantle source composition, there is little or no evidence for upwelling mantle plume activity in the region. On the other hand, pure-shear stretching, exemplified by 'pull-apart' rifting, is interpreted as the principal cause of lithospheric thinning, leading to passive mantle upwelling and decompression melting.

(6) Assuming a regional lithosphere thickness of c. 80 km and average heat flow of 75 mW/m^2 (i.e., a geotherm of c. 4C/100m), estimated mantle potential temperature (Tp) of about 1400°C exceeds those associated with ambient, stable continental lithosphere (1350°C). Such elevated temperature, coupled with a lithosphere stretching factor (β) > 1.5, is sufficient for decompression melting to account for the observed extent of regional monogenic volcanism.

Acknowledgments

This study is financially supported by the international collaborative project, coded QTRU06.04/24-26 (No.24-47-04001), of the Vietnam Academy of Science and Technology, to whom the authors gratefully acknowledge their support. Two anonymous reviewers are thanked for their constructive criticism and suggestions, which helped clarify the manuscript. We thank Prof. Phan Trong Trinh for his helpful editorial handling of the manuscript.

Reference

Anderson D.L., 1994. The sublithospheric mantle as the source of continental flood basalts: the case against the continental lithosphere and plume head reservoirs. Earth and Planetary Science Letters, 123, 269–280.

Anderson D.L., 1995. Lithosphere, asthenosphere, and perisphere. Reviews of Geophysics, 33, 125–149.

Bui H.H., Fyhn M.B.W., Hovikoski J., Boldreel L.O., Tuan N.Q., Dam M.H., Long H.V., Tung N.T., Nielsen L.H., Abatzis I., 2023. Cenozoic structural development of the western flank of the Song Hong Basin, Gulf of Tonkin, Vietnam: Linking with onshore strike-slip faulting and regional tectonics. Journal of Asian Earth Sciences, 246, 105581. https://doi.org/10.1016/j.jseaes.2023.105581.

Castillo P.R., MacIsaac C., Perry S., Veizer J., 2018. Marine carbonates in the mantle source of oceanic basalts: Pb isotopic constraints. Scientific Reports, 8, 14932. Doi: 10.1038/s41598-018-33178-4.

Cung T.C., Dorobek S., Richter C., Flower M., Kikawa E., Nguyen Y.T., McCabe R., 1998. Paleomagnetism of late Neogene basalts in Vietnam and Thailand: Implications for the Tertiary tectonic history of Indochina. In: M.F.J. Flower, S.-l. Chung, T.-y. Lee and C.-h. Lo (Editors), Mantle Dynamics and Plate Interactions in East Asia. Am. Geophys. Union, Geodynamics Series, 27, 289–300.

Danyushevsky L.V., Plechov P., 2011. Petrolog3: Integrated software for modeling crystallization processes. Geochemistry, Geophysics, Geosystems, 12(7). Doi.org/10.1029/2011GC003516.

Davidson J., Turner S., Plank T., 2013. Dy/Dy*: Variations arising from mantle sources and petrogenetic processes. Journal of Petrology, 34(3), 525–537. Doi: 10.1093/petrology/egs076.

Flower M.F.J., Tamaki K., Hoang N., 1998. Mantle extrusion: a model for dispersed volcanism and DUPAL-like asthenosphere in East Asia and the WPAC. In: M.F.J. Flower, S.L. Chung, C.H. Lo, eds. Mantle Dynamics and Plate Interactions in East Asia. Geodynamics Series. Washington, DC: American Geophysical Union, 27, 67–88.

Flower M.F.J., Russo R.M., Tamaki K., Hoang N., 2001. Mantle contamination and the Izu-Bonin-Mariana (IBM) 'high-tide mark': evidence for mantle extrusion caused by Tethyan closure. Tectonophysics, 333, 9–34.

Frey F.A., Clague D., Mahoney J.J., Sinton J.M., 2000. Volcanism at the edge of the Hawaiian plume:

petrogenesis of submarine alkalic lavas from the North Arch volcanic field. Journal of Petrology, 41(5), 667–691.

Fyhn M.B.W., Hoang B.H., Cuong T.D., Tuan N.Q., Schmidt W.J., Boldreel L.O., Anh N.T.K., Huyen N.T., Trinh X.C, 2020. Paleogene structural development of the northern Song Hong Basin and adjacent areas: Implications for the role of extrusion tectonics in basin formation in the Gulf of Tonkin. Tectonophysics, 789, 228522. https://doi.org/10.1016/j.tecto.2020.228522.

Gaetani G.A., Grove T.L., 1998. The influence of water on melting of mantle peridotite. Contrib. Miner. Petrol., 131, 323–346.

Gill J.B., 1981. Orogenic Andesite and Plate Tectonics. Springer-Verlag, New York, 330p.

Harry D.L., Leeman W.P., 1995. Partial melting of melt metasomatized subcontinental mantle and the magma source potential of the lower lithosphere. Journal of Geophysical Research, 100(B6), 10255–10269. https://doi.org/10.1029/94JB03065.

Hart S., 1984. DUPAL anomaly: a large scale isotopic anomaly in the southern hemisphere. Nature, 309, 753–756.

Hart S., 1988. Heterogeneous mantle domains: signatures, genesis and mixing chronologies. Earth and Planetary Science Letters, 90, 273–296.

Herzberg C., Zhang J., 1996. Melting experiments on anhydrous peridotite KLB-1: compositions of magmas in the upper mantle and transition zone. J. Geophys. Res., 101, 8271–8295.

Hirschmann M.M., Kogiso T., Baker M.B., Stolper E.M., 2003. Alkalic magmas generated by partial melting of garnetpyroxenite. Geology, 31, 481–484.

Hirose K., Kushiro I., 1993. Partial melting of dry peridotites at high pressures: determination of composition of melts segregated from peridotite using aggregate of diamond. Earth and Planetary Science Letters, 114, 477–489.

Hoang N., 2023. Miocene-Quaternary basaltic volcanism in Vietnam. Natural Science and Technology Publishing House, VAST, Hanoi, 372p.

Hoang N., Flower M.F.J., 1998. Petrogenesis of Cenozoic basalts from Vietnam: implication for origins of a “diffuse igneous province”. Journal of Petrology, 39(3), 369–395. https://doi.org/10.1093/petroj/39.3.369.

Hoang N., Huong T.T., Shinjo R., Le D.A., Le D.L., Phan D.P., 2025. Geochemistry of late Miocene-Pleistocene basalts from a coastal area of Vietnam: Implication for small-scale mantle heterogeneities. Journal of Asian Earth Sciences, 281, 106488, https://doi.org/10.1016/j.jseaes.2025.106488.

Hoang N., Shinjo R., Huong T.T., Le D.L., Le D.A., 2021. Mantle geodynamics and source domain of the East Vietnam Sea opening-induced volcanism in Vietnam and neighboring regions. Vietnam Journal of Marine Science and Technology, 21(4), 393–417. https://doi.org/10.15625/1859-3097/16856.

Hoang N., Shinjo R., La T.P., Le D.A., Huong T.T., Zoltán Pécskay, Dao Thai Bac, 2019. Pleistocene basalt volcanism in the Krông Nô area and vicinity, Dak Nong province (Vietnam). J. Asian Earth Sciences, 181, 103903. https://doi.org/10.1016/j.jseaes.2019.103903.

Hoang N., Shinjo R., Le D.L., Huong T.T., Tran V.A., Phan D.P., Pham T.D., Cu S.T., Nguyen T.T., Le T.P.D., 2024. Pleistocene basaltic volcanism in the southeastern Ailao Shan - Red River Shear zone: Implications for the injection of metasomatized asthenospheric mantle under the region. Vietnam Journal of Earth Sciences, 47(1), 16–43. https://doi.org/10.15625/2615-9783/21539.

Hofmann A.W., 1988. Chemical differentiation of the earth: the relationship between mantle, continental crust, and oceanic crust. Earth and Planetary Science Letters, 90, 297–314.

Holm P.M., 2002. Sr, Nd and Pb isotopic composition of in situ lower crust at the Southwest Indian Ridge: results from ODP Leg 176. Chemical Geology, 184, 195–216.

Hong-Anh H.T., Choi S.H., Yu Y.-j., Pham T.H., Nguyen K.H., Ryu J.-S., 2018. Geochemical constraints on the spatial distribution of recycled oceanic crust in the mantle source of late Cenozoic basalts. Vietnam. Lithos, 296–299, 382–395.

Huong T.T., Hoang N., 2018. Petrology, geochemistry, and Sr, Nd isotopes of mantle xenolith in Nghia Dan alkaline basalt (West Nghe An): implications for lithospheric mantle characteristics beaneath the region. Vietnam Journal of Earth Sciences, 40(3), 207–27. https://doi.org/10.15625/0866-7187/40/3/12614.

Ignat'ev A.V., Velivetskaya T.A., Budnitskii S.Yu., 2010. A method for determining argon isotopes in a continuous helium flow for K/Ar geochronology. Journal of Analytical Chemistry, 65, 1347–1355.

Ionov D.A., O'Reilly S.Y., Griffin W.B., 1998. A geotherm and lithospheric section for central Mongolia (Tariat region). In: M.F.J. Flower, S.-l. Chung, T.-Y. Lee and C.-H. Lo (Editors), Mantle Dynamics and Plate Interactions in East Asia. American Geophysical Union, Geodynamics Series, 127–153.

Jolivet L., Faccenna C., Becker T., Tesauro M., Sternai P., Bouilhol P., 2018. Mantle flow and deforming continents: From India-Asia convergence to Pacific subduction. Tectonics, 37, 2887–2914. https://doi.org/10.1029/2018TC005036.

Jones R.E., van Keken P.E., Hauri E.H., Tucker J.M., Vervoort J., Ballentine C.J., 2019. Origins of the terrestrial Hf-Nd mantle array: Evidence from a combined geodynamical-geochemical approach. Earth Planet Sci. Lett., 518, 26–39.

Kimura J.-I., Yoshida T., 2006. Contributions of slab fluid, mantle wedge and crust to the origin of Quaternary lavas in the NE Japan arc. Journal of Petrology, 47(11), 2185–2232.

Kushiro I., 1996. Partial melting of a fertile mantle peridotite at high pressure: An experimental study using aggregates of diamond. In: A. Basu and S.R. Hart (Editors), Earth Processes: Reading the Isotopic Code. Geophys. Monogr. 95, American Geophysical Union, 109–122.

Kushiro I., 1998. Compositions of partial melts formed in mantle peridotites at high pressures and their relation to those of primitive MORB. Physics of the Earth and Planetary Interiors, 107, 103–110.

Latin D., White N., 1990. Generating melt during lithospheric extension: Pure shear vs. simple shear. Geology, 18, 327–331.

Le Bas M.J., Le Maitre R.W., Streckeisen A., Zanettin B., 1986. A Chemical Classification of Volcanic Rocks Based on the Total Alkali-Silica Diagram. Journal of Petrology, 27, 745–750. https://doi.org/10.1093/petrology/27.3.745.

Le D. Anh, Hoang N., Shakirov R., Huong T.T., 2017. Geochemistry of late miocene-pleistocene basalts in the Phu Quy island area (East Vietnam Sea): Implication for mantle source feature and melt generation. Vietnam Journal of Earth Sciences, 39(3), 270–288. https://doi.org/10.15625/0866-7187/39/3/10559.

Lee T.-Y., Lo C.-H., Chung S.-L., Chen C.-Y., Wang P.-L., Lin W.-P., Hoang N., Cung T.C., Nguyen T.Y., 1998. $^{40}Ar/^{39}Ar$ dating result of Neogene basalts in Vietnam and its tectonic implication. In: M.F.J. Flower, C-h. Lo, S-l. Chung, T. Lee (Editors) Mantle Dynamics and Plate Interactions in East Asia. AGU Monograph, 27, 317–330.

Liu D., Zhao Z., Zhu D-Ch., Niu Y., DePaolo D.J., T. Harrison M., Mo X-X., Dong G., Zhou S., Sun C., Zhang Z., Liu J., 2014. Post collisional potassic and ultrapotassic rocks in southern Tibet: Mantle and crustal origins in response to India-Asia collision and convergence. Geochimica et Cosmochimica Acta, 143, 207–231.

Mahoney J.J, Graham D.W., Christie D.M., Johnson K.T.M., Hall S.L., Vonderhaar D.L., 2002. Between a hotspot and a cold spot: Isotopic variation in the Southeast Indian Ridge asthenosphere, 86E-118E. Journal of Petrology, 43(7), 1155–1176.

Mayle M., Harry D.L., 2023. Syn-rift magmatism and sequential melting of fertile lithologies in the lithosphere and asthenosphere. Journal of Geophysical Research: Solid Earth, 128, e2023JB027072. https://doi.org/10.1029/2023JB027072.

McDonough W.F., Sun, S.-S., 1995. The composition of the Earth. Chemical Geology, 120, 223–253.

McKenzie D., Bickle, M.J., 1988. The volume and composition of melt generated by extension of the lithosphere. Journal of Petrology, 26, 625–679.

McKenzie D., Stracke A., Blichert-Toft J., Albarède F., Grönvold K., O'Nions R.K., 2004. Source enrichment processes responsible for isotopic anomalies in oceanic island basalts. Geochimica et Cosmochimica Acta, 68(12), 2699–2724.

McLennan S.M., 2001. Relationships between the trace element composition of sedimentary rocks and upper continental crust. Geochemistry, Geophysics, Geosystems, 2, 2000GC000109.

Modreski P.J., Boettcher A.L., 1973. Phase relationships of phlogopite in the systems K_2O-MgO-CaO-Al_2O_3-SiO_2-H_2O to 35 kilobars: a better model for micas in the interior of the earth. American Journal of Science, 273, 385–414.

Neal C.R., Mahoney J.J., Chazey III W.J., 2002. Mantle sources and the highly variable role of continental lithosphere in basalt petrogenesis of the Kergulen Plateau and Broken Ridge LIP: Results from ODP Leg 183. J. Petrol, 43(7), 1177–1205.

Nguyen H.H., Carter A., Hoang L.V., Fox M., Pham S.N., Vinh H.B., 2022. Evolution of the continental margin of south to central Vietnam and its relationship to opening of the East Vietnam Sea. Tectonics, 41, e2021TC006971. https://doi.org/10.1029/2021TC006971.

Nguyen N.T., Phan T.H., Bui V.N., Nguyen T.T.H., Tran T.L., 2018. Moho depth of the northern Vietnam and Gulf of Tonkin from 3D inverse interpretation of gravity anomaly data. Journal of Geophysics and Engineering, 15, 1651–1662. https://doi.org/10.1088/1742-2140/aabf48.

Nguyen N.T., Bui V.N., Nguyen T.T.H., Than D.L., 2014. Application of power density spectrum of magnetic anomaly to estimate the structure of magnetic layer of the earth crust in the Bac Bo Gulf. Vietnam Journal of Marine Science and Technology, 14(4A), 137–148. https://doi.org/10.15625/1859-3097/14/4A/6040 (in Vietnamese with English abstract).

Pham T.L., Do D.T., Oksum E., Le T.S., 2019. Estimation of Curie point depths in the Southern Vietnam continental shelf using magnetic data. Vietnam Journal of Earth Sciences, 41(3), 216–228. https://doi.org/10.15625/0866-7187/41/3/13830.

Phan T.T., Ngo V.L., Nguyen V.H., Hoang Q.V., Bui V.T., Bui P.T., Mai T.T., Hoang N., 2012. Late Quaternary tectonics and seistmotectonics along the Red River fault zone, North Vietnam. Earth-Science Reviews, 114(3–4), 224–235. https://doi:10.1016/j.earscirev.2012.06.008.

Phung V.P., Anh L.D., Hanh N.T.H., Golozubov V.V., Kasatkin S., 2023. Tectonic evolution of the Red River basin and adjacent area (Vietnam) in Cenozoic era. Vietnam Journal of Marine Science and Technology, 23(4), 345–359. https://doi.org/10.15625/1859-3097/18583.

Prytulak J., Elliot T., 2007. TiO_2 enrichment in ocean island basalts. Earth Planet Sci. Lett., 263(3–4), 388–403.

Putirka K., 2008. Thermometers and Barometers for Volcanic Systems. In: Putirka, K., Tepley, F. (Eds.), Minerals, Inclusions and Volcanic Processes, Reviews in Mineralogy and Geochemistry, Mineralogical Soc. Am., 69, 61–120.

Rangin C., Klein M., Roques D., Le Pichon X., Trong L.V., 1995. The Red River fault system in the Tonkin Gulf, Vietnam. Tectonophysics, 243(3–4), 209–222.

Regelous M., Niu Y., Wendt J.I., Batiza R., Greig A., Collerson K.D., 1999. Variations in the geochemistry if magmatism on the East Pacific Rise at 10°30'N since 800 ka. Earth and Planetary Science Letters, 168, 45–63.

Richard N., Burberry C.M, Hoang N., Le D.A., Dinh Q.S., Elkins L.J., 2024. Neogene-Recent Reactivation of Pre-Existing Faults in South-Central Vietnam, With Implications for the Extrusion of Indochina. Tectonics, 43, e2023TC008231. https://doi.org/10.1029/2023TC008231.

Roeder P.L., Emslie R.F., 1970. Olivine-liquid equilibria. Contributions to Mineralogy and Petrology, 29, 275–289.

Rudnick R.L., Fountain D.M., 1995. Nature and composition of the continental crust: a lower crustal perspective. Reviews of Geophysics, 33(3), 267–309.

Tapponnier P., Lacassin R., Leloup P.H., Schärer U., Zhong D., Liu X., Ji S., Zhang L., Zhong J., 1990. The Ailao Shan-Red River metamorphic belt: Tertiary left-lateral shear between Indochina and South China. Nature, 343, 431–437.

Tapponnier P., Peltzer G., Dain A.Y., Armijo R., Cobbold P., 1982. Propagating extrusion tectonics in Asia: New insights from simple experiments with plasticine. Geology, 10(12), 611–616.

Tatsumi Y., 1989. Migration of fluid phases and genesis of basalt magmas in subduction zones. Journal of Geophysical Research, 94, 4697–4707.

Taylor S.R., McLennan S.M., 1981. The composition and evolution of the continental crust: rare earth element evidence from sedimentary rocks. Philosophical Transactions of the Royal Society of London, 301, 381–399.

Tenner T.J., Hirschmann M.M., Humayun M., 2012. The effect of H_2O on partial melting of garnet peridotite at 3.5 GPa. Geochem. Geophys. Geosyst., 13. http://dx.doi.org/10.1029/2011GC003942 (Q03016).

Tran D.T., Le D.A., Tran D.L., Trinh T.M.T., Nguyen T.M.H., 2017. Position resources in Con Co Island. Vietnam Journal of Marine Science and Technology, 17(1), 12–22 (in Vietnamese with English abstract). Doi: 10.15625/1859-3097/17/1/8406.

Tu K., Flower M.F.J., Carlson R.W., Xie G., Chen C.-Y., Zhang M., 1992. Magmatism in the South China Basin: 1. Isotopic and trace-element evidence for an endogenous Dupal mantle component. Chemical Geology, 97(1–2), 47–63. http://dx.doi.org/10.1016/0009-2541(92)90135-R.

Turner S., Hawkesworth C., 1995. The nature of the sub-continental mantle: constraints from the major element composition of continental flood basalts. Chemical Geology, 120, 295–314.

White W.M., Hofmann A.W., Puchelt H., 1987. Isotope geochemistry of Pacific mid-ocean ridge basalt. Journal of Geophysical Research, 92(B6), 4881–4893.

Wilson M., 1993. Magmatism and the geodynamics of basin formation. Sedimentary Geology, 86, 5–29.

Yamashita S., Tatsumi Y., 1994. Thermal and geochemical evolution of the mantle wedge in the northeast Japan arc. 2. Contribution from geochemistry. Journal of Geophysical Research, 99(B11), 22285–22293. https://doi.org/10.1029/94JB00282.

Yan Q-S., Shi X., Metcalfe I., Liu S., Xu T., Kornkanitnan N., Sirichaiseth, Yuan L., Zhang Y., Zhang H., 2018. Hainan mantle plume produced late Cenozoic basaltic rocks in Thailand, Southeast Asia. Scientific Report. Doi: 10.1038/s41598-018- 20712-7.

Yu C., Shi X., Yang X., Zhao J., Chen M., Tang Q., 2017. Deep thermal structure of Southeast Asia constrained by S-velocity data. Marine Geophys. Res., 38, 341–355. Doi: 10.1007/s11001-017-9311-x.

Zhang Y-S., Tanimoto T., 1993. High-resolution global upper mantle structure and plate tectonics. Journal of Geophysical Research, 98, 9793–9823.

SUPPLEMENTARY FILES

Sample preparation and analytical procedures

Sample preparation

The sample preparation for petrographic, geochemical, and isotopic analysis was described in Hoang et al. (2025), but is briefly given here. Approximately 100 grams of basalt were crushed into chips. These chips were hand-picked to remove visible xenoliths or secondary materials, such as carbonate minerals. The selected chips were ultrasonically cleaned in 250 ml Pyrex jars filled with clean water for about one hour, with several rinses to ensure thorough cleaning. They were then boiled in Milli-Q in a clean oven for at least 24 hours at 110°C, during which the water was replaced multiple times.

Once thoroughly dried, the samples were pounded in a clean steel mill to a 1–2 mm grain size. About 15 grams of each sample were then finely ground for subsequent analyses.

Loss on ignition (LOI) was determined using the following procedure: about 2 grams of the ground sample were placed in clean 10 ml ceramic crucibles and heated at ~100°C for 1 hour to remove surface moisture. The crucibles were then heated to 950°C for 3 hours to drive off post-eruption matters and volatile components. These treated powders were later used for trace element and isotope analyses.

In addition, some samples from Con Co Island and coastal sites such as Vinh Moc, which were apparently interacted with seawater, underwent acid-leaching before isotope analysis. For leaching, weigh 60 mg of powdered samples in 15 ml Teflon beakers, multiple rinse with Millipore water. After drying at 100°C, the samples were treated with 5 ml of double distilled 6 M HCl and warmed on a hotplate at approximately 65°C for 2 hours. The acid-leaching step eliminated alteration-induced minerals and any post-eruption contaminants. The leached samples were then multiple rinsed Millipore water and dried for analysis.

Analytical methods

A set of samples from Gio Linh and the surrounding area were analyzed for K-Ar dating at the Far East Geological Institute (Vladivostok), using Ignat'ev et al. (2010)'s procedure. The newly obtained and previously published age data are shown in Table 1 (Lee et al., 1998; Cung et al., 1998).

The major element analysis:

Major element contents were determined from glass beads by a Rigaku ZSX Primus II X-ray fluorescence spectrometer (XRF) at the University of the Ryukyus, Japan. Calibration lines were constructed using geological standards from the Geological Survey of Japan (GSJ) and the United States Geological Survey (USGS). Standards BHVO-2 and JB-1a were repeatedly analyzed for the analytical accuracy's verification. The major element compositions are listed in Table 1.

The trace and minor element analysis:

For trace element analysis, approximately 50 mg of heated sample were placed into 15 ml Teflon bottles, then treated with double distilled HNO_3 and HF, with the concentration of 68% and 48%, respectively, on a hotplate at 130°C for about 48 hours to secure proper dissolution. After completely dried, 3 ml of 2 M HNO_3 were weighed in, and the samples were left overnight on a hotplate at low temperature to achieve equilibrium. The resulting solution were diluted in 10 ml of 0.3M HNO_3 to reach a dilution factor at 4000 ±0.0005 for mass spectrometry.

The trace and minor element concentrations were acquired from a Neptune Elemental Q-ICP-MS at the University of the Ryukyus. Samples were analyzed three times; the values were averaged to calculate the standard deviations ($\pm 1\sigma$). Standards BHVO-2 and JB-1a were routinely analyzed among the samples to ensure data repeatability and validity. Trace element results are presented in Table 1.

Table 1. Age data, geochemical and isotope compositions of basalts from North Central Vietnam

No	DACC-1	DACC-2	DA-8	2014f-B	2014f-C	DA-22	DA-23	DA-24	DA-25	DA-20	DA-18	DA-17	9/85-KS
Location	**Con Co**	**Con Co**	**Vinh Moc**	**Vinh Moc**	**Gio Linh**	**Gio Linh**	**Gio Linh**	**Gio Linh**	**Gio Linh**	**Dong Ha**	**Dong Ha**	**Khe Sanh**	**Khe Sanh**
Latitude (N)	17°08'16"	17°09'05"	17°05'6"	17°4'08"	16°54'21"	16°55'11"	16°54'59"	16°56'53"	17°56'56"	15°46'16"	16°46'18"	16°38'04"	16°38'04"
Longitude (E)	107°19'50"	107°20'40"	107°04'14"	107°6'19"	107°02'40"	107°00'30"	106°58'30"	107°01'47"	107°01'18"	106°55'30"	106°55'40"	106°46'48"	106°46'48"
Age (mill. years)	0.36 ±0.08*	0.36 ±0.08*	1.32 ±0.28**	0.56 ±0.07**	1.3 ±0.11†	1.3 ±0.11†	1.3 ±0.11†	1.32 ±0.11†	1.3 ±0.11†	-	-	4.5 ±0.22*	4.5 ±0.22*
SiO_2	50.34	52.27	50.98	51.94	50.59	50.81	51.12	50.42	50.56	50.85	50.58	46.14	47.19
TiO_2	2.35	2.26	2.03	2.16	1.91	1.89	2.13	1.92	1.93	2.21	2.29	2.81	2.61
Al_2O_3	15.46	14.78	14.06	15.18	15.91	14.21	15.14	14.25	14.22	15.16	15.19	13.71	14.22
Fe_2O_3	1.68	1.58	1.62	1.58	1.63	1.64	1.65	1.71	1.67	1.60	1.64	1.82	1.58
FeO	9.51	8.97	9.20	8.96	9.21	9.28	9.33	9.68	9.47	9.04	9.28	10.34	8.96
MnO	0.15	0.14	0.13	0.14	0.14	0.14	0.18	0.17	0.14	0.14	0.14	0.17	0.15
MgO	5.73	5.24	7.54	5.67	7.12	7.90	5.82	7.16	8.15	5.95	5.64	8.55	8.39
CaO	8.69	8.10	7.75	7.87	7.59	7.86	7.18	8.01	7.74	7.80	7.23	9.35	9.2
Na_2O	3.37	3.53	3.64	3.57	3.84	3.65	3.89	3.37	3.66	3.94	3.91	3.33	3.01
K_2O	1.07	1.65	1.54	1.77	1.25	1.28	1.67	1.10	1.15	1.81	1.88	1.91	1.5
P_2O_5	0.39	0.40	0.40	0.48	0.29	0.35	0.45	0.31	0.32	0.51	0.51	0.59	0.53
LOI				0.35	0.26								2.21
Total	98.74	98.92	98.89	99.32	99.74	99.00	98.57	98.09	98.99	99.01	98.28	98.72	99.55
Mg#	51.8	51.0	59.4	53.0	57.9	60.3	52.7	56.9	60.6	54.0	52.0	59.6	62.5
K(Fe-Mg)	0.28	0.29	0.21	0.27	0.22	0.20	0.27	0.23	0.20	0.26	0.28	0.20	0.18
Fo (olivine)	78.2	77.7	83.0	79.0	82.1	83.5	78.8	81.5	83.7	79.6	78.3	83.1	84.8
Li (ppm)	30.13	55.26	22.04	2.52	7.73	27.64	33.39	38.45	43.23	15.04	12.39	5.41	-
Be	2.48	3.74	3.20	1.36	1.45	2.46	3.55	3.61	3.46	2.35	1.85	0.31	-
Sc	34.71	41.67	35.75	8.22	-	28.97	33.56	46.60	55.34	21.88	15.30	2.09	-
V	305.30	248.30	235.40	164.01	177.02	228.70	267.80	315.20	323.40	173.90	171.10	191.70	-
Cr	82.43	197.10	427.40	198.86	293.33	117.50	197.40	161.40	126.30	464.10	248.60	312.70	-
Co	45.27	36.65	46.07	30.17	-	49.01	45.70	71.46	59.43	39.27	39.72	53.03	-
Ni	60.16	41.42	118.00	64.47	133.25	142.70	88.41	252.00	176.60	76.99	80.83	163.30	134
Rb	20.48	48.06	41.23	47.7	33.5	34.12	47.53	27.31	33.74	44.90	53.48	46.26	29
Sr	539.90	509.30	549.50	517.8	482.5	567.20	654.20	573.30	609.70	620.10	578.10	933.20	787
Y	32.72	28.82	22.07	16.08	23.28	21.01	23.75	32.02	22.89	32.73	35.82	20.65	20
Zr	187.60	175.00	163.10	144.98	119.83	133.90	175.10	138.10	143.80	214.80	220.10	205.00	122
Nb	35.20	33.90	34.43	35.44	26.52	28.08	41.07	27.42	28.26	44.60	46.55	56.46	38
Cs	0.56	1.47	0.24	0.01	0.70	0.84	0.35	0.30	0.78	0.13	0.36	0.75	-
Ba	402.60	390.20	389.70	315.46	312.22	341.60	568.00	337.10	347.60	496.70	509.70	469.00	481
La	26.26	24.30	22.82	22.94	18.58	19.57	27.78	20.58	19.86	36.86	34.01	34.82	24.9
Ce	48.38	45.92	44.91	45.71	35.04	37.03	56.60	38.11	38.67	65.69	61.84	65.31	60.8
Pr	6.44	5.90	5.69	5.33	4.17	4.75	6.77	5.05	4.96	8.17	7.90	7.89	-
Nd	26.63	24.16	23.31	23.26	18.61	19.75	27.39	21.06	20.72	31.84	31.22	30.50	25.9
Sm	6.78	6.14	5.70	5.36	4.57	4.91	6.62	5.42	5.29	7.10	7.07	6.56	5.6
Eu	2.09	1.88	1.77	1.91	1.59	1.57	2.10	1.79	1.71	2.26	2.20	2.06	2
Gd	6.38	5.66	4.94	5.54	4.82	4.34	5.63	5.17	4.66	6.54	6.54	5.52	-
Tb	0.99	0.88	0.74	0.78	0.69	0.65	0.83	0.79	0.71	0.96	0.97	0.75	-
Dy	5.52	4.94	4.01	3.90	3.82	3.63	4.48	4.47	3.88	5.35	5.41	3.92	-
Ho	0.91	0.81	0.65	0.69	0.71	0.59	0.72	0.76	0.64	0.90	0.92	0.61	-
Er	2.52	2.27	1.81	1.79	1.84	1.62	1.95	2.12	1.78	2.54	2.61	1.67	-
Tm	0.34	0.32	0.25	0.21	0.24	0.22	0.27	0.28	0.24	0.35	0.36	0.22	-
Yb	2.07	1.91	1.53	1.26	1.40	1.36	1.65	1.70	1.48	2.15	2.13	1.30	1.8
Lu	0.31	0.28	0.22	0.17	0.20	0.20	0.24	0.26	0.22	0.32	0.32	0.19	0.3
Hf	4.07	3.83	3.57	3.32	2.96	2.91	3.64	2.99	3.09	4.14	4.37	3.91	3.6
Ta	2.13	2.08	2.16	1.75	1.66	1.72	2.44	1.66	1.73	2.81	2.91	3.54	2.4
Pb	4.78	5.69	3.69	4.30	3.25	3.46	3.85	3.24	4.14	4.82	4.54	4.25	-
Th	4.73	4.56	4.24	3.38	3.40	3.53	4.89	3.38	3.56	5.77	6.07	5.30	1.8
U	0.75	1.18	1.09	0.60	0.75	0.83	1.25	0.81	0.97	0.88	1.48	0.98	-
La/Yb	12.66	12.72	14.91	18.14	13.24	14.37	16.86	12.10	13.46	17.14	15.97	26.76	13.83
$^{87}Sr/^{86}Sr$ *(unleached)*				0.705875	0.704711	0.704833							
±2σe				0.000010	0.000008	0.000009							
$^{87}Sr/^{86}Sr$ *(leached)*				0.705101	0.704678	0.704725							
2σe				0.000007	0.000008	0.000006							
$^{87}Sr/^{86}Sr$ *(baked)*	0.705090	0.705070	0.705045	0.705084	0.704649	0.704702	0.704711	0.704675	0.704604	0.704726	0.704700	0.703940	0.704084
±2σe	0.000007	0.000006	0.000007	0.000008	0.000006	0.000005	0.000006	0.000008	0.000006	0.000009	0.000008	0.000005	0.000006
$^{143}Nd/^{144}Nd$ *(unleached)*				0.512687	0.512671	0.512681							
±2σe				0.000005	0.000004	0.000006							
$^{143}Nd/^{144}Nd$ *(leached)*				0.512698	0.512671	0.512701							
±2σe				0.000006	0.000007	0.000006							
$^{143}Nd/^{144}Nd$ *(baked)*	0.512682	0.512695	0.512716	0.512700	0.512681	0.512713	0.512721	0.512754	0.512711	0.512751	0.512745	0.512833	0.512819
±2σe				0.000004	0.000006	0.000005							
ε_{Nd}	0.86	1.11	1.53	1.21	0.85	1.46	1.63	2.27	1.43	2.21	2.08	3.81	3.53
$^{206}Pb/^{204}Pb$ *(unleached)*				18.824	18.844	18.830							
±2σe				0.0003	0.0005	0.0010							
$^{206}Pb/^{204}Pb$ *(leached)*				18.748	18.828	18.808							
±2σe				0.0004	0.0006	0.0004							
$^{206}Pb/^{204}Pb$ (baked)	18.803	18.701	18.764	18.742	18.814	18.793	18.830	18.808	18.802	18.782	18.770	18.673	18.776
±2σe	0.0006	0.0004	0.0007	0.0001	0.0005	0.0002	0.0004	0.0005	0.0005	0.0007	0.0004	0.0003	0.0005
$^{207}Pb/^{204}Pb$ *(unleached)*				15.722	15.763	15.747							15.635
±2σe				0.0005	0.0001	0.0005							
$^{207}Pb/^{204}Pb$ *(leached)*				15.682	15.731	15.719							
±2σe				0.0008	0.0003	0.0002							
$^{207}Pb/^{204}Pb$ (baked)	15.731	15.716	15.704	15.680	15.716	15.710	15.719	15.720	15.717	15.708	15.700	15.611	15.635
	0.0005	0.0007	0.0004	0.0003	0.0005	0.0007	0.0001	0.0005	0.0002	0.0004	0.0005	0.0006	0.0004
$^{208}Pb/^{204}Pb$ *(unleached)*				39.199	39.269	39.347							
±2σe				0.0024	0.0019	0.0009							
$^{208}Pb/^{204}Pb$ *(leached)*				39.027	39.145	39.177							
±2σe				0.0017	0.0021	0.0018							
$^{208}Pb/^{204}Pb$ *(baked)*	39.322	39.154	39.120	39.020	39.140	39.168	39.236	39.208	39.195	39.265	39.233	38.887	39.050
±2σe	0.0014	0.0008	0.0020	0.0022	0.0024	0.0012	0.0024	0.0008	0.0016	0.0010	0.0016	0.0022	0.0010
$^{176}Hf/^{177}Hf$ *(baked)*	0.282893	0.282895	0.282892	0.282886	0.282893	0.282890	0.282886	0.282876	0.282898	0.282871	0.282885	0.282973	0.282961
±2σe	0.000006	0.00001	0.00001	0.000008	0.000007	0.00001	0.000006	0.000012	0.00001	0.000008	0.000008	0.00001	0.000007
ε_{Hf}	3.80	3.90	3.78	3.57	3.82	3.70	3.56	3.22	3.98	3.05	3.54	6.65	6.22

Note: $\varepsilon_{Nd} = (((^{143}Nd/^{144}Nd_{sample}/0.512638_{CHUR})-1)*10000$, $\varepsilon_{Hf} = (((^{176}Hf/^{177}Hf_{sample}/0.282785_{CHUR})-1)*10000$; Age data (*) from Lee et al. (1998), (**) from Cung et al. (1998), (†) this study

The Sr, Nd, Hf, and Pb isotopic measurements:

For isotopic data acquisition, approximately 50 mg of heated samples were placed in 15- or 7-mL Teflon bottles with triple-distilled HF and HNO_3 (2:1 ratio, and concentrations at 48% and 68% respectively) and on a hot plate at ~130°C for two days. Samples were evaporated properly, 1.6 mL of 2.75 M HNO_3 were added to the dried residues and centrifuged, ready for chromatographic separation.

Approximately 15 mg of dissolved sample (~0.5 ml) was taken for the cation exchange chromatography. A 50 µL-Eichrom Sr-spec resin bed in 1 mL quartz column was employed to separate strontium and lead metals, using, respectively, weak HNO_3 and concentrated HCl. Hafnium and neodymium metals were separated using 1-mL Eichrom Ln resin bed in 10 mL cleaned Nalgene columns. Hf was collected using mixtures of 2 M HCl with 0.2 M HF and neodymium was extracted by 0.2 M HCl.

Strontium, neodymium, hafnium, and lead Isotope ratios were acquired from a Neptune Plus MC-ICP-MS at University of the Ryukyus. Selected samples were re-analyzed by a NU Plasma 3 MC-ICP-MS at the Institute of Earth Sciences (VAST) to confirm data validity and evaluate acid-leaching's effects.

During Sr isotope measurement, instrumental mass fractionation was normalized to $^{86}Sr/^{88}Sr = 0.1194$, and data were presented relative to the value of $^{87}Sr/^{86}Sr = 0.710255 \pm 0.000015$ (2σ, n = 128) of the NBS 987 standard. Interference from ^{84}Kr and ^{85}Rb was minimized through optimized instrument settings. For neodymium isotopes, fractionation was referred to $^{146}Nd/^{144}Nd$ at 0.7219, and values were referenced to the JNdi-1 standard, which yielded $^{143}Nd/^{144}Nd = 0.512116 \pm 0.000013$ (2σ, n = 122). The hafnium isotopic ratios ($^{176}Hf/^{177}Hf$) were referenced relative to the value of $^{176}Hf/^{177}Hf = 0.282136$ of the JMC475 standard (Wiedenbeck et al., 1995). For Pb isotopes, the NBS 981 standard yielded 16.938 ± 0.0006, 15.493 ± 0.0005, and 36.704 ± 0.0016 (2σ, n = 88), respectively, for $^{206}Pb/^{204}Pb$, $^{207}Pb/^{204}Pb$, and $^{208}Pb/^{204}Pb$. Procedural blanks ranged from 50 to 100 pg Pb, which is negligible for samples containing >200 ng purified Pb.

Table 2. Compositions of the *computed primitive melts* of the North Central Vietnam basalts

Sample ID*	SiO_2	TiO_2	Al_2O_3	Fe_2O_3	FeO	MnO	MgO	CaO	Na_2O	K_2O	P_2O_5	Total	$Fo_{(Ol)}$	T°C (1)	T°C (2)	Pkb (3)
DACC-1	48.41	1.74	11.38	1.21	10.69	0.12	15.91	7.05	2.44	0.77	0.28	100	90.0	1371.9	1393.8	17.6
DACC-2	49.99	1.69	11.05	1.16	10.03	0.11	15.02	6.87	2.59	1.21	0.29	100	90.1	1354.8	1362.9	11.1
DA-8	49.50	1.66	11.52	1.33	9.89	0.11	14.98	6.45	2.98	1.26	0.32	100	90.0	1355.1	1356.5	13.1
DA-18	48.96	1.73	11.42	1.21	10.33	0.11	15.52	6.05	2.90	1.39	0.38	100	90.1	1365.5	1377.0	15.3
DA-20	49.10	1.70	11.67	1.21	9.94	0.12	14.91	6.59	3.00	1.37	0.38	100	90.0	1354.1	1359.0	14.7
DA-21	49.28	1.62	11.53	1.32	9.93	0.12	15.10	6.56	3.04	1.17	0.32	100	90.1	1357.1	1358.2	14.0
DA-22	49.34	1.57	11.75	1.35	9.94	0.12	15.06	6.50	3.02	1.06	0.29	100	90.0	1356.6	1358.7	13.8
DA-23	49.33	1.62	11.50	1.23	10.29	0.15	15.37	6.01	2.92	1.25	0.34	100	90.0	1362.7	1374.9	13.8
DA-24	49.07	1.52	11.30	1.35	10.49	0.14	15.81	6.55	2.66	0.87	0.24	100	90.0	1369.9	1384.5	14.9
DA-25	49.14	1.59	11.71	1.38	10.08	0.12	15.39	6.37	3.01	0.95	0.26	100	90.1	1362.6	1365.5	14.6
DA-17	45.44	2.26	11.07	1.47	10.89	0.14	16.46	7.55	2.69	1.54	0.48	100	90.0	1383.3	1403.1	29.6

(*)The sample coordinates are as in Table 1; $Fo_{(ol)}$: forsteristic content of calculated olivine in equilibrium with the primitive melts (after Putirka, 2008); (1) melting temperatures calculated using the method of Danyushevsky and Plechov (2011), (2) melting temperatures and pressures (3) estimated using formulas given in Hoang and Flower (1998)